Reflectance spectroscopy for diagnosis of precancerous changes in human epithelium

by

Vadim Backman

M.S.
St. Petersburg State Technical University
(1996)

SUBMITTED TO THE DEPARTMENT OF PHYSICS
IN PARTIAL FULFILLMENT OF THE
REQUIREMENTS FOR DEGREE OF
MASTER OF SCIENCES IN PHYSICS

at the
Massachusetts Institute of Technology
January 1998

Signature of Author: _____
Department of Physics
January 21, 1998

Certified by: _____
Michael S. Feld
Professor, Department of Physics
Thesis Supervispor

_____
Lev T. Perelman
Principal Research Scientist, Department of Physics
Thesis Co-Supervisor

Accepted by: _____
George F. Koster, Chairman
Departmental Graduate Committee

Reflectance spectroscopy for diagnosis of early precancerous changes in human epithelium

by

Vadim Backman

Submitted to the Department of Physics on January 21, 1998 in partial fulfillment of the requirements for the Degree of Master of Science in Physics

ABSTRACT

This thesis discusses observation of a fine structure component in light backscattered from mucosal tissue which oscillates in wavelength. This structure is ordinary masked by a diffusive background. We have identified the origin of this component as being due to light which is Mie-scattered by surface epithelial nuclei.

We developed a model describing light propagation in turbid biological media and its interaction with epithelium, which is the uppermost tissue layer, resulting in modulation of the reflectance from tissue. This oscillatory fine structure was observed in the reflectance spectra from cell monolayers simulating real tissues and esophagus of human subjects.

By analyzing the amplitude and frequency of the fine structure, the density and size distribution of epithelial cell nuclei can be extracted. These quantities are important indicators of early precancerous changes in biological tissues. Enlarged nuclei are primary indicators of cancer and dysplasia in most human tissues. At the same time, if diagnosed at this stage, cancer is curable in about 90% cases. Thus, the ability to measure nuclear size distribution *in-vivo* (inside the body) has valuable applications and can be used as a tool to diagnose early precancerous changes in the human body non-invasively and in real time.

Thesis Supervisors: Michael S. Feld, Ph.D.

Title: Professor, Department of Physics

Thesis Co-Supervisor:Lev T. Perelman, Ph.D.

Title: Principal Research Scientist

ACKNOLEDGEMENTS

The author sincerely thanks his research advisors Prof. Michael S. Feld and Dr.Lev T. Perelman for their scientific guidance, support, and personal attention. Without their guidance and active participation in the research the project would not be started, proceeded, and completed.

The author thanks all the members of George R. Harrison Spectroscopy Laboratory for their friendship, and support. Special thanks to Dr. Irving Itzkan for his advising on the experimental work, George Zonios for his help, support and patience, and Dr. Michael Wallace for his friendship and optimism.

Additional thanks to Dr. Richard Mitchell, Harvard Medical School, for introducing me to the world of pathology, histology, and physiology. The knowledge I gained from his lectures helped me greatly in this research.

Special thanks to my family. My work on this project, studying in MIT, higher and secondary school education, and my whole existence would not be possible without them.

Table of Contents

Chapter 1

Introduction

1.1 Optical techniques in medicine

Biomedical optics is a rapidly growing field that uses optical techniques for the purposes of biology and medicine. Biomedical optics can be divided into biological optics, which studies fundamental properties of the biological molecules, cells, and tissues, and medical optics, which uses optical methods either non-invasively or invasively.

Invasive applications employ the "effect of light on tissue" [1]. Invasive applications can be classified by type of changes light induces in the tissue: mechanical, chemical, or thermal. Major applications include laser ablation [2-4] (mechanical changes), photodynamic therapy [5] (chemical changes), and laser hyperthermia [6] (thermal changes). Generally speaking, laser ablation uses short high power pulses of laser light. They result in removal of the irradiated tissue. An important modification of this technique uses laser induced shock waves to ablate the tissue with minimal effect on the surrounding tissues [4]. This results in clean minimally invasive surgical intervention. Photodynamic therapy uses laser light to generate toxic chemicals from endogenous or exogenous molecules that mark a diseased tissue. This results in cellular necrosis and tissue destruction. Laser hyperthermia uses light to increase tissue temperature and induce thermal shock that again leads to cellular necrosis and tissue destruction.

Non-invasive or minimally invasive applications employ the "effect of tissue on light" [1]. A tissue under study is irradiated by a light source. Then reflected or transmitted light is collected and analyzed. Thus, some tissue attributes can be revealed. These attributes may be (1) multicellular properties (architectural disorganization, changes in surface morphology, cell crowding), (2) cellular properties (enlargement and hyperchromaticity of cell nuclei, increased concentration of organelles), and (3) molecular (shift of NADH, NADPH to oxidized states, decreased activity of ferrochelatase, presence of abnormal proteins).

Non-invasive or minimally invasive applications of medical spectroscopy can be divided "imaging applications'' (2D and 3D, the latter are based on the photon migration approach [7] and are usually characterized by deep penetration depths), and "diagnostic applications" ("spectral pathology" [8]). There are three major types of diagnostic spectroscopy: reflectance spectroscopy, laser-induce fluorescence spectroscopy (LIFS), and Raman spectroscopy.

In reflectance spectroscopy a portion of tissue is irradiated by white light and light reflected from the tissue is collected. Since light propagation in tissue is governed by two processes – elastic scattering and absorption – the reflected signal can bring information about these tissue properties. This, in tern, can give information about particular types of tissue absorbers (hemoglobin for example) and scatterers (extracellular matrix, mitochondria, cell nuclei, etc.). Thus, reflectance spectroscopy is best suited to detect architectural multicellular and intracellular changes. (These are the same tissue characteristics that a pathologist is looking at when analyzing a biopsy slide under a microscope – he does not do chemical or genetic analysis but rather is looking for intra- and multicellular architectural changes.) It has being applied to measure blood oxygenation [9], tissue oxygenation [10], and detect precancerous changes in several organs such as colon, esophagus, etc. [10].

While reflectance spectroscopy is best suited to detect architectural changes, two other types of tissue spectroscopy – LIFS and Raman spectroscopy – can measure molecular changes. LIFS uses a monochromatic laser source to illuminate the tissue, and the fluorescence signal at the wavelengths longer than that of the illumination beam is

collected. The signal may be 10^3 times weaker than that of reflectance. LIF signals depend not only on the scattering and absorptive properties of the tissue, but also on the presence of endogenous fluorophores such as collagen, NADH, and porphyrins. Unfortunately, not all types of tissues contain such fluorophores in amounts sufficient to measure their fluorescence (epithelial cells, for example, are known to have weak fluorescence). LIFS was applied to detect atherosclerosis of aorta and coronary artery [11], dysplasia in colon and bladder [12], adenomatous polyps in colon [13], and cancers in other organs such as esophagus [14] and breast [15].

Raman spectroscopy measures a frequency shift created by the vibrations of the molecules within the tissue. The signal is very weak – 10^6-10^9 times weaker than that of the elastic scattering. This technique is well suited to measure the chemical composition of the tissue. The drawback of this technique is the length of time necessary to collect a signal. With technological advances, some of these difficulties are being solved and Raman spectroscopy can find a broad application in clinical medicine in the future. Raman spectroscopy has being studied as a tool to diagnose breast cancer, atherosclerosis, etc. [16].

1.2 Reflectance spectroscopy as a diagnostic tool

1.2.1 Diagnosis of precancerous changes

Early diagnosis of cancer and precancerous (dysplastic) changes is a key element in the treatment of cancer. Current diagnostic methods employ techniques based on X-ray, CT scan, MRI, and ultrasound. While different in many aspects, all these methods have one thing in common – they cannot diagnose microscopic lesions at an early stage, when such lesions can easily be effectively treated (not to mention a great variety of precancerous conditions which are not identifiable with these methods at all, such as flat dysplasia in Barrett's esophagus and ulcerative colitis). The only way we can look at tissues at a microscopic scale is by taking biopsy. Probably, biopsy is still the best way to

diagnose most disease. However, it is invasive (requires tissue removal), and can give very high sample error (consider the probability to find a flat dysplastic lesion 0.1-0.5 cm in diameter in the colon, if one can take reasonable number of biopsies 0.01 cm^2 each). Many studies have being performed to find a technique to diagnose diseases of microscopic dimensions (μm's-mm's) screening large tissue areas, in-real-time, *in-vivo*, and non-invasively. Such a technique would give a number of procedure-oriented advantages (non-invasive, substitutes a number of other procedures and services – cheaper and faster) and result-oriented advantages (screening of large tissue areas, in real time and *in-vivo* – possibility to diagnose and treat the disease at the same time, targeting of the diseased areas – limit surgical interventions).

For the last decade extensive investigations have been performed to find a substitute for random biopsy, in order to provide accurate diagnosis of dysplasia in different organs. Optical techniques are well suited for this purpose, since they are non-invasive, do not require tissue removal, and can be performed *in-vivo*. Moreover, they are fast (can be applied in real time), relatively cheap, and they are able to work in microscopic dimensions, which can allow one to search for very small dysplastic sites, which are frequently missed by random biopsies. While most human organs can be diagnosed by means of optical techniques, such techniques are especially applicable to the gastrointestinal tract, since it is easily accessible by optical probes, which can be inserted into one of the channels of a conventional endoscope. We shall refer to gastrointestinal precancerous changes throughout this manuscript.

1.2.2 Optical techniques to diagnose precancerous changes

One of the difficulties in diagnosing dysplasia in the gastrointestinal tract lies in the fact that these changes are confined to the epithelial layer, which can be as thin as 20μm, one cell layer, and relatively transparent to optical radiation. At the same time, a fluorescence or reflectance spectrum is mostly formed in deeper tissue layers. In spite of this, such optical techniques as LIFS and reflectance spectroscopy have been applied to

diagnose dysplastic changes. For example, LIFS was used to diagnose high-grade dysplasia in Berrett's esophagus [14], colonic polyps [13], and bladder cancer [12]. LIFS is well suited to reveal biochemical alterations in the tissue. If the cells or stroma of the diseased tissue accumulate any fluorophores that are not present in a healthy tissue, the presence of such fluorophores can be detected by LIFS. A few endogenous fluorophores were proposed to accumulate in dysplastic cells. Several studies have shown increased concentrations of protoporphyrins in malignant cells (cancer and high grade dysplasia) [14]. However, these studies did not show such increase in tissues with low-grade dysplasia. This may mean that low-grade dysplastic cells either do not accumulate measurable amounts of these fluorophores or do not accumulate them at all. The last alternative is supported by the "multiple hit theory", proven to be correct for a number of types of cancer (colon adenocarcinoma, retinoblastoma, etc.). This theory suggests that a number of genetic alterations are necessary to transform a normal cell to malignant one, i.e. a number of genes have to be altered. Moreover, mutation in one gene may result in predisposition of another gene being mutated as well (however the last hypothesis has yet to be proven). The first mutation is usually in a gene responsible for cell proliferation and/or apoptosis (programmed cell death). The lesions composed of such cells usually remain intact and can not lead to metastasis directly. These cells do not show changes in chemical composition, but they proliferate more rapidly and, therefore, have increased nuclei, nucleoli, and exhibit some intracellular architectural changes. A technique capable of diagnosing a disease at this stage should be able to detect changes in cellular architecture rather than provide chemical analysis of the tissue. At the next stage of disease, another genetic mutation may lead to cell redifferentiation. This is a sign of malignancy. These cells can show some alterations in their chemical composition.

At some point, a precancerous lesion initiates angiogenesis (growth of new blood vessels to support the lesion). This process is absolutely necessarily for a tumor to continue to grow and, eventually, to produce metastasis. It has not being explained yet why and how some tumors switch to angiogenesis. Angogenic tumors can grow uncontrollably. At this stage, because of the increased blood supply, protoporphyrins are

accumulated in malignant cells and can be detected by some spectroscopic technique such as LIFS.

1.2.3 Reflectance spectroscopy to diagnose early precancerous changes

One of the most prominent features of a dysplastic epithelium is the presence of enlarged, hyperchromatic, stratified, and crowded nuclei [18]. In fact, these changes in nuclear size and spatial distribution are among the main markers used by a pathologist to diagnose a tissue as dysplastic. Reflectance spectroscopy is well suited to detect inrtracellular architectural changes. Light scattering in tissue has being considered as one of the main difficulties of biomedical spectroscopy. Indeed, scattering prevents photons from propagating in straight trajectories, and results in randomization of the photons inside the tissue. When a photon is collected, one has little information about its origin and path. Therefore, great deal of research is being done to diminish the effect of scattering in order to perform "absorption" or "transmission" spectroscopy (analogy with X-ray imaging).

At the same time, scattering might be useful. Different cellular and intracellular structures have distinctive scattering patterns. Changes in intracellular architecture (enlarged nuclei or the number of mitochondria, for example) can result in a different scattering pattern of the tissue. This can be determined with reflectance ("scattering spectroscopy"). Another difficulty of the application of reflectance spectroscopy to diagnose dysplasia is that the changes we need to detect are limited to a thin surface layer (20-30μm, see section 1.2.2). However, as discussed below, this fact can be used to advantage, as well. (Thus, one can *use* the difficulties that biological media present instead of trying to *eliminate* them.)

The primary scattering centers in biological tissue are thought to be the collagen fiber network of the extracellular matrix, the mitochondria, and other intracellular

substructures, all with dimensions smaller than optical wavelengths [23]. However, larger structures, such as cell nuclei, typically 5-15 μm in diameter, can also scatter light.

Single scattering of collimated light has been used widely to study cells and subcellular structures in suspensions [18]. In tissues this approach can not be used since light is randomized by multiple scattering. However, diffusely scattered light from tissue contains information about underlying structures [19]. Transmitted [20] and backscattered [10] photons can be used. However, this information is averaged at least over several transport lengths because of the randomization. On the other hand, the light in the thin layer near the tissue surface is not randomized completely, and information about individual scatters can be retained even if the layer thickness is significantly smaller than a transport length. Our goal, therefore, is to find a way to detect changes in a single scattering pattern and use this information to characterize scatterers in a thin near surface layer by analyzing the reflectance spectrum. This thesis is devoted to addressing this problem [21].

1.3 Organization of the thesis

This thesis reports observation of a fine structure component in backscattered light from biological tissue which oscillates in wavelength. This structure is ordinarily masked by a diffusive background. We have identified the origin of this component as being due to light which is Mie-scattered by surface epithelial cell nuclei. By analyzing the amplitude and frequency of the fine structure, the density and size distribution of these nuclei can be extracted. These quantities are important indicators of precancerous changes in biological tissue.

The thesis consists of three parts. Chapter 2 theoretically predicts the oscillatory component in reflectance from biological tissue covered by a thin layer that has a rich cellular content (epithelium). It starts with the discussion of single scattering events. Scatterers that are large relative to the wavelength of the scattered light are considered. The problem of light scattering by a spherical particle of arbitrary size was solved by

Gustav Mie in 1907 [22]. However, the solutions for the cross section and phase function are not applicable analytically and allow only numerical interpretation. This work presents another approach. The WKB approximation is applied to determine the scattering characteristics of large particle scattering. This approximation was first used to calculate the optical cross section of a large particle by Van de Hulst [23]. This work introduces the WKB approximation to estimate the scattering phase function for forward and backward scattering. Analytical solutions are obtained and discussed. It is shown that scattering characteristics have oscillatory wavelength dependence.

Multiple scattering by a slab of large particles is considered next. It is shown that the signal of light backscattered from such a slab and light transmitted through it exhibits a oscillatory component similar to that of the cross section. Section 2.3 shows that analysis of this oscillatory component allows to determine the size distribution of the scatterers inside the slab.

Chapter 3 presents an experimental study of the oscillatory component. The oscillatory component was observed in reflectance from tissue phantoms, cellular monolayers, and in esophageal tissues of human subjects. Experiments with tissue phantoms, cellular monolayers and clinical experiments are described. It is shown that the technique has a potential to diagnose early precancerous changes.

Chapter 4 summarizes the main results of the work and discusses future directions.

References

1. J.A. Parrish, and B.C. Wilson, Photochem. Photobio., **53**, 731 (1991).
2. J. Seeger, and G.S. Adela, Surg. Annu., **22**, 299 (1990).
3. J. Dixon, *Surgical Applications of Lasers*, Year Book Publisher, Chicago (1987).
4. I. Itzkan, D. Albagli, M.L. Dark, L.T. Perelman, C. von Rosenberg, M.S. Feld, PNAS, **92**, 1960 (1995).
5. T.J. Dougherty, Oncology, **3**, 67 (1989).
6. L.J. Anghilery, and J. Robert, *Hyperthermia in Cancer Treatment*, CRC Press, Boca Raton (1986).
7. L.T. Perelman, J. Wu, I. Itzkan and M.S. Feld, Phys. Rev. Lett. **72**, 1341 (1994).
8. G. Zonios, R. Cothren, J.M. Crawford, M. Fitzmaurice, R. Manoharan, J. Van Dam, M.S. Feld, Ann. New York Acad. Sci., in press (1998).
9. L.C. Reynolds, C. London, and a. Ishimaru, App. Opt., **15**, 2059 (1976).
10. G. Zonios, L.T. Perelman, V. Backman, R. Manoharan, J. Van Dam, and M.S. Feld (to be published).
11. R. Richards Kortum, R.P. Rava, M. Fitzmaurice, L.L. Tong, N.B. Ratliff, J.R. Kramer, and M.S. Feld, IEEE Trans. Biomed. Eng., **36**, 1222 (1989).
12. R.M. Cothren, R. Richards-Kortum, M.V. Sivak, etc., Gastro. Endo., **36**, 105 (1990).
13. G.I. Zonios, R.M. Cothren, J.T. Arendt, J. Wu, J. Van Dam, J.M. Crawford, R. Manoharan, and M.S. Feld, IEEE Trans. Biomed. Eng., **43**, 113 (1996).
14. T. Vo-Dinh, M. Panjehpour, B.F. Overholt, etc., Laser. Surg. Med., **16**, 41 (1996).
15. R.R. Alfano, A. Pradham, G.C. Tang, and S.J. Wahl, J. Opt. Soc. Am. B, **6**, 1015 (1989).
16. R. Manoharan, Y. Wang, M.S. Feld, Spectrochim. Act. A, **52**, 215 (1996).
17. R.S.Cotran, S.L. Robbins, V. Kumar, *Robbins Pathological Basis of Disease* (W.B. Saunders Company, Philadelphia, 1994).

18. M. R. Melamed, T. Lindmo, M. L. Mendelsohn, *Flow Cytometry and Sorting* (Wiley-Liss, New York, 1990).

19. J.R. Mourant, T. Fuselier, J. Boyer, T.M. Johnson, and I. Bigio, Appl. Opt. **36**, 949 (1997).

20. P. D. Kaplan, A. D. Dinsmore, A.G. Yodh, and D. J. Pine, Phys. Rev. E **50**, 4827, (1994).

21. L.T. Perelman, V. Backman, M. Wallace, G. Zonios, R. Manoharan, A. Nusrat, S. Shields, M. Seiler, C. Lima, T. Hamano, I. Itzkan, J. Van Dam, J.M. Crawford, and M.S. Feld, Phys.Rev. Lett., **80**, 627 (1998).

22. G. Mie, Annalen der Physik, Band 25, No3 (1908).

23. H.C. van de Hulst, *Light Scattering by Small Particles* (Dover Publications, New York, 1957).

24. A.G. Yodh and B. Chance, Physics Today, **48**(3), 34 (1995).

Chapter 2

Theoretical prediction of oscillatory fine structure in the reflectance from biological tissue

2.1 Light scattering by large particles

In the field of biomedical spectroscopy, tissue is usually considered to be a turbid medium. These media are spatially inhomogeneous. Thus, the amplitudes and phases of electromagnetic waves propagating through such media fluctuate randomly in space and time. The description of the interaction of light with biological tissues is essentially the problem of interaction of light with a random medium. A number of ways to describe light propagation in random media have being developed. (1) Transport theory, in which the propagation of light specific intensity through a random distribution of scattering and absorptive particles is studied using the transport equation [1] and phase effects are neglected.(2) Multiple scattering theory, which incorporates field equations and statistical considerations [2,3]. This theory includes phase effects. However, in practice, it is impossible to obtain a formulation which includes scattering, absorption, diffraction, interference, etc., and in all such theories the solutions are approximate. Twersky's, Dyson's, and Bethe-Salpeter's theories are examples [1,2,4]. (3) Numerical approaches, such as the Monte Carlo method [5]. These methods try to simulate a physical experiment by a computer simulation or "numerical experiment". While different in many respects, all these approaches have one fact in common. They consider the light interaction with a multiple particle system on the basis of understanding of how light interacts with a single particle. A system can consist of great variety of particles of different

sizes, shapes, refractive indexes, etc.; still we can apply any of these approaches only if know how any of the particles would scatter and/or absorb light.

Our main interest is in the light propagation in an epithelial layer containing cell nuclei of different sizes. Epithelial nuclei are spheroidal Mie scatters with refractive index higher than that of the surrounding cytoplasm [6,7]. Normal nuclei have a characteristic diameter l=4-7 μm. In contrast, dysplastic nuclei can be as large as 20 μm in height, occupying almost the entire cell volume [8]. As shown below, light scattering by the nuclei gives rise to a oscillatory component in the reflectance from the tissue. First, we consider a single nucleus and examine its scattering characteristics. Second, we consider the contributions from many nuclei (slab of nuclei). Throughout this chapter we consider only the optical properties of cell nuclei. Moreover, most of the results presented here are quite general and applicable to many other types of scatterers. Thus, we will refer to cell nuclei as "scattering particles" in most cases.

When a single particle is illuminated by a light wave, part of the incident radiation is absorbed and another part is scattered. This scattering is described by the scattering amplitude [10]. Two important optical characteristics of a particle can be defined using the scattering amplitude. One is its cross section. The scattering cross section, σ_s, is defined as the cross section of a particle which would produce amount of scattering equal to the total observed scattered power at all directions, and is given by [9]

$$\sigma_s = \int_{4\pi} |f(\mathbf{s},\mathbf{s}')|^2 d\mathbf{s}', \tag{2.1}$$

where $\mathbf{s}$ is the unit vector in the direction of propagation of the initial wave and $f(\mathbf{s},\mathbf{s}')$ is the amplitude of the scattered wave in the far field in direction $\mathbf{s}'$. The absorption cross section σ_a is defined as the cross section of a totally absorbing particle which would absorb the amount of power absorbed by the particle. The sum of the scattering and absorption cross sections is called the total cross section

$$\sigma_t = \sigma_s + \sigma_a \tag{2.2}$$

Since experiments show that cell nuclei have negligible absorptive properties, we concentrate on their scattering characteristics.

Another important characteristic is the phase function p(s,s′), which is proportional to the probability of a photon to be scattered by the particle from direction **s** to **s′** [1]. We will normalize it in such a way that its integral over all possible directions, **s′**, equals unity:

$$p(\mathbf{s},\mathbf{s}')=\sigma_s^{-1}\left|f(\mathbf{s},\mathbf{s}')\right|^2,\quad \int_{4\pi} p(\mathbf{s},\mathbf{s}')d\mathbf{s}'=1. \tag{2.3}$$

Considering that a cell nucleus is a particle large comparing to an optical wavelength, we shall study the properties of the cross section and phase function of a large particle in the following sections. We shall then apply our knowledge of a single scattering event to describe reflectance from a multiparticle system (slab of nuclei), which is a physical representation of the epithelial layer covering surface of the tissue.

2.1.1 Scattering cross section of a large particle

In the scalar wave approximation, interaction of light with any particle is nothing but the scattering of a plane wave on some energy potential. If the particle is uniform, the energy potential is a square well. When the scatterer is large relative to the wavelength, we can apply eikonal or WKB approximations [9,10]. The latter is valid if the following condition is satisfied:

$$\frac{\Delta U l}{hc} >> 1 \tag{2.4}$$

with ΔU the energy difference and l the characteristic size of the potential well. When a photon of wavelength λ is scattered by a spherical particle of diameter l, we have $\Delta U = hc\left(n_2 - n_1\right)/\lambda$, with n_2 and n_1 refractive indexes of the particle and the surrounding medium, respectively. Condition (2.4) can be rewritten as follows:

$$\frac{l(n_2 - n_1)}{\lambda} >> 1 \tag{2.5}$$

If the particle is large enough to satisfy (2.5), the WKB approximation is applicable. In optics the WKB approximation is usually referred to as the Van de Hulst approximation [11]. We will use the latter terminology.

The path length of the light ray that passes through the particle is [11]

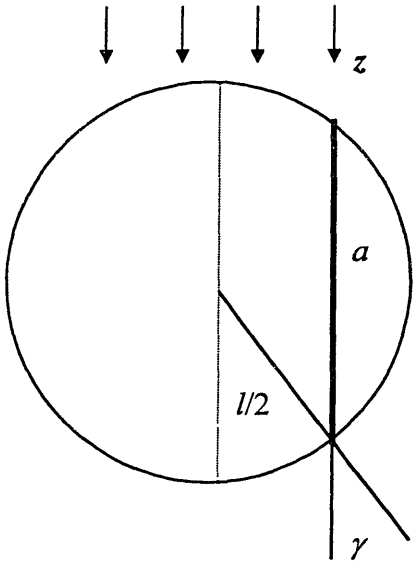

Figure 2.1. Angle γ.

$$a = l\cos\gamma\,, \tag{2.6}$$

with γ the angle between the radial direction and the direction of the initial ray (Fig. 2.1). The phase of the wave in this direction is shifted from exp(*ikz*), with *k* the wavenumber, to

$$\exp(ikz + ik(n_2 - n_1)l\cos\gamma) \quad . \tag{2.7}$$

At a large distance from the particle one observes a superposition of the initial wave and the scattered one. Thus, the observed beam differs from the incident by

$$f(\mathbf{s},\mathbf{s})E_i e^{ikz}\,2\pi ik^{-1} = \int dS\left(e^{2ix(n_2-n_1)\cos\gamma} - 1\right)E_i e^{ikz} \tag{2.8}$$

where $x = \frac{\pi l}{\lambda}$, E_i is the amplitude of the incident wave, $dS = 2\pi\cos\gamma d\cos\gamma$, and the integration is taken over the cross section of the particle. According to the optical theorem [9], the total cross section of a particle that has rotational-reflection symmetry is proportional to the imaginary part of the scattering amplitude in the forward direction:

$$\sigma_t \approx \frac{4\pi}{k}\mathrm{Im}\,f(\mathbf{s},\mathbf{s})\,. \tag{2.9}$$

Therefore,

$$\sigma_t \approx 2\,\mathrm{Re}\int dS\left(1 - e^{2ix(n_2-n_1)\cos\gamma}\right). \tag{2.10}$$

Noting that

$$\int_0^1 y\left(1-e^{-ty}\right)dy = \frac{1}{2}+\frac{e^{-t}}{t}+\frac{e^{-t}-1}{t^2}, \tag{2.11}$$

and assuming the particle and the medium to be nonabsorbing (Im n_2= Im n_1=0), one can obtain the expression for the total cross section [9]:

$$\sigma_t \approx \frac{\pi l^2}{2}\left\{1-\frac{\sin\left(2x(n_2-n_1)\right)}{x(n_2-n_1)}+\left(\frac{\sin\left(x(n_2-n_1)\right)}{x(n_2-n_1)}\right)^2\right\} \quad . \tag{2.12}$$

As we will see, this expression plays one of the central roles in the thesis.

The cross section (2.12) depends on the size of the scatterer, the wavelength, and the difference in refractive indexes. We further note that the ratio of the optical cross section to the geometrical cross section of the particle, the so called efficiency parameter, is a function of $\zeta=x(n_2-n_1)$. The functional dependence of σ_t on ζ is shown in Fig. 2.2.

The cross section (2.12) was obtained using the approximation valid for large particles. It is *quantitatively* accurate only if $\zeta>>1$. However, it shows behavior of σ_t which is *qualitatively* correct for any ζ. When ζ is small, (2.12) equals to the large ζ limit of the Rayleigh-Gans theory [12]. When $\zeta>>1$,

$$\sigma_t \approx \frac{\pi l^2}{2}. \tag{2.13}$$

A large sphere blocks out twice its geometrical cross sectional area. This fact, known as the extinction paradox [11], contradicts the intuitive understanding that if a light beam is scattered by a very large particle, the photons do not "feel" the particle boundaries, and, therefore, the cross section should equal the geometrical cross sectional area of the scatterer that is predicted by the geometrical optics limit. The qualitative explanation of this paradox is that one factor $\pi l^2/4$ represents cross sectional area of the particle and the other $\pi l^2/4$ comes from diffraction of light around the edges.

Another important property of σ_t that will be used later on is the presence of the maxima and minima (Fig.2.2). We shall refer to this structure as the "oscillatory component". The physical cause of this oscillatory behavior is interference between the refracted and diffracted waves. Fig. 2.3 shows the wavelength dependence of σ_t for particles of different

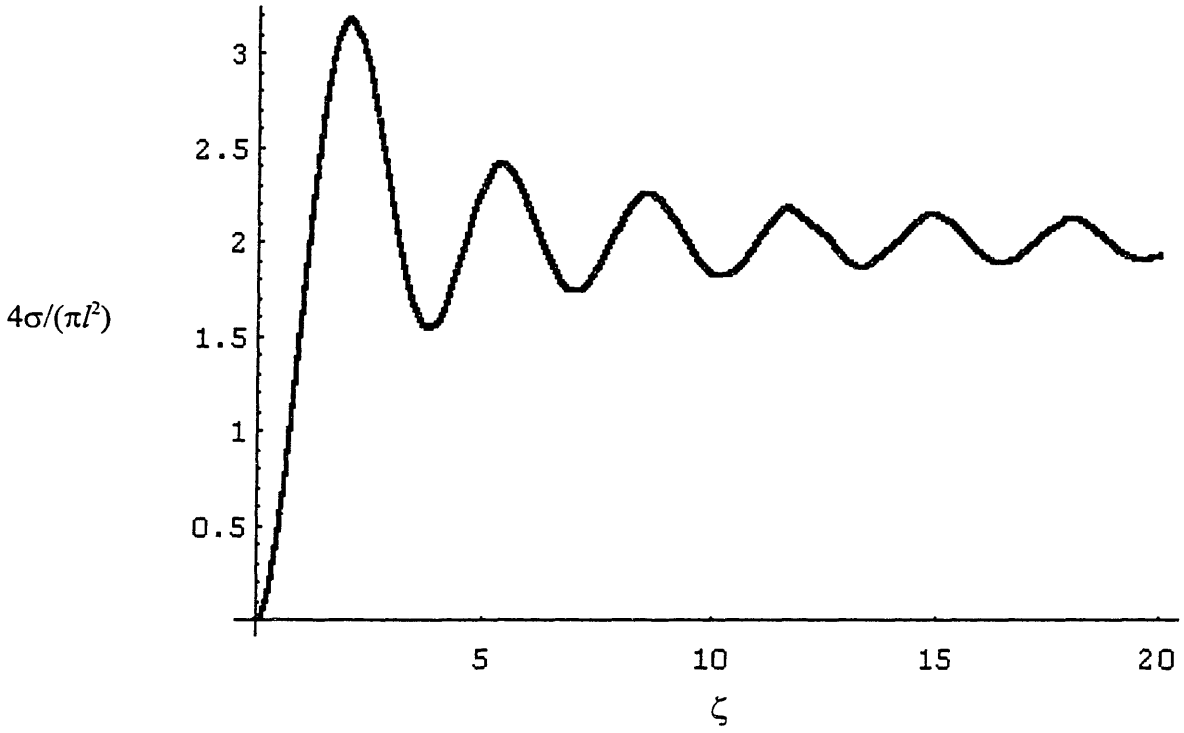

Figure 2.2 Total cross section σ as a function of ζ.

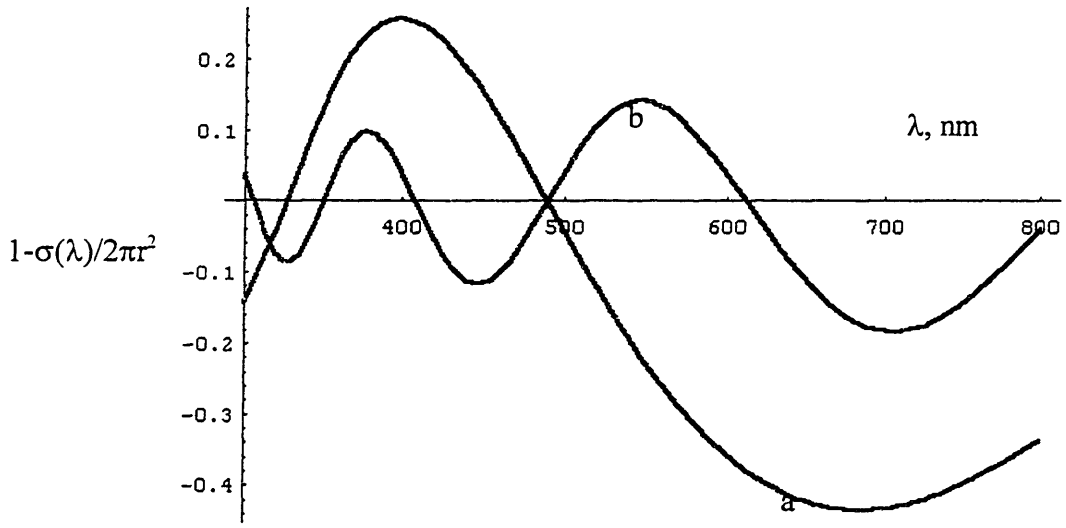

Figure 2.3 Oscillatory component of the cross section of particles with refractive index 1.06 and two different diameters: (a) l=5μm; (b) l=15μm.

sizes. The periodicity of this component is proportional to the diameter of the particle and the difference in refractive indexes. In other words, the larger and denser the scatterer, the higher the periodicity. Thus, if one can measure the wavelength dependence of the cross section, one can determine size of the particle by analyzing the oscillatory component.

One more comment about the cross section should be made. We assumed the particle to be nonabsorbing (Im n_2=0). This assumption is valid for many important scattering systems, including cell nuclei, because they consist mostly of water, DNA and proteins, all of which are known to have negligible absorption in the optical region. Thus, the calculated total cross section σ_t exactly equals the scattering cross section σ_s. However, this is not the case if the particle is absorbing and the imaginary part of its refractive index is not zero. In this case one can easily find the expression for the absorption cross section:

$$\sigma_a \approx 2\,\mathrm{Re}\int dS\left(1-e^{-4x\,\mathrm{Im}\,n_2\cos\gamma}\right), \tag{2.14}$$

which for small $x\mathrm{Im}n_2$ reduces to

$$\sigma_a \approx \tfrac{2}{3}\pi l^2 x\,\mathrm{Im}n, \tag{2.15}$$

and for both $x\mathrm{Im}n_2$ and ρ large,

$$\sigma_a \approx \sigma_s \approx \tfrac{1}{4}\pi l^2. \tag{2.16}$$

This simply means that the absorption cross section of a large particle equals to its geometrical cross section (which is one of the definitions of a black body). In the following we confine our attention to particles with negligible absorption, and therefore can use expression (2.12).

2.1.2 Scattering phase function of a large particle

To completely describe single scattering, knowledge of the cross section is not sufficient. We need to know the probability of a photon to be scattered in a particular direction, which is described by the phase function (2.3). The exact solution of the scattering of a plane electromagnetic wave by an isotropic, homogenous sphere was obtained by Mie in 1908 [13]. The expressions for the cross section and the phase function generated by this

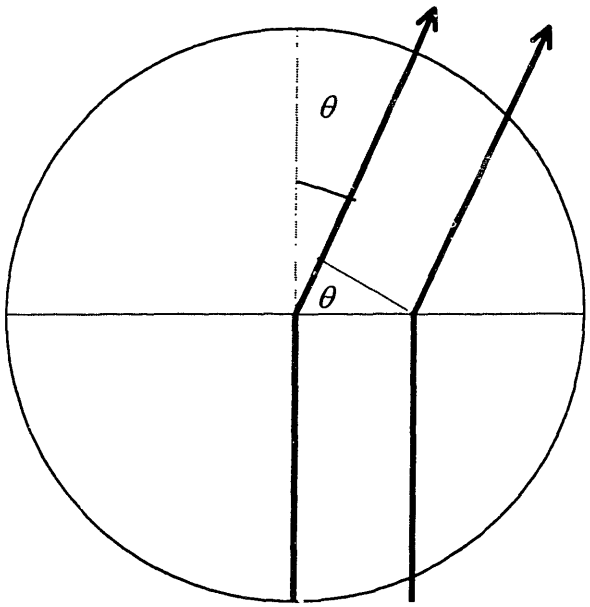

Figure 2.4. δ is the phase shift between the two light rays shown.

theory can be found elsewhere [1]. The solutions are mathematically complicated and do not allow simple physical interpretation. To calculate the value of the cross section or phase function, extensive computations are necessary. Moreover, mathematical transformations such as integration of a phase function over some angle range can only be done numerically.

Since we are interested in the scattering by large particles, we can obtain an approximate expression for the phase function using the Van de Hulst approximation, without employing Mie theory. To do this, we first find the scattering amplitude. Again, we assume the particle to be rotationally-reflectionally symmetrical and homogenous. It was already mentioned that a large particle scatters light predominantly in the forward direction. This intuitively obvious fact can be derived from the optical theorem in the general case [9].

We can estimate the scattering amplitude in the forward direction using (2.9):

$$|f(\mathbf{s},\mathbf{s})| \geq \frac{k}{4\pi}\sigma_t \tag{2.17}$$

and

$$\frac{|f(\mathbf{s},\mathbf{s})|^2}{\sigma_s} \geq \left(\frac{k}{4\pi}\right)^2 \sigma_t \,. \tag{2.18}$$

At the same time

$$\sigma_s = \int_{4\pi} ds' |f(\mathbf{s},\mathbf{s}')|^2 = \int_0^{2\pi} d\varphi \int_{-1}^{1} d\cos\theta |f(\theta)|^2 \geq 4\pi |f(\mathbf{s},\mathbf{s})|^2 \sin^2 \frac{\theta_f}{2}, \tag{2.19}$$

where θ and φ are polar angles determining direction $\boldsymbol{s}'$ relative to the direction of the incident wave $\boldsymbol{s}$, and θ_f is the angular width of the forward peak. Using inequality (2.18), we obtain [9]

$$\sin^2 \frac{\theta_f}{2} \leq \frac{4\pi}{k^2 \sigma_t} . \tag{2.20}$$

As mentioned in the previous section, the total cross section of a large particles is twice its geometrical cross sectional area. For such a particle $k^2\sigma_t >> 1$ and the angular width can be estimated by

$$\theta_f \leq \frac{2\lambda}{\sqrt{\pi\sigma_t}} \approx \frac{\lambda}{l} . \tag{2.21}$$

Thus, a large particle scatters light predominately in the forward direction. However, as will be shown in section 2.1.2.2, such particles have a backward directed scattering peak as well. First we determine the approximate expression for the phase function for small angle scattering (see expresion 2.27). Backward scattering will be considered in section 2.1.2.2 (see expression 2.34)

2.1.2.1 Small angle scattering

Consider a spherical particle with diameter l. Because of the symmetry, both the scattering amplitude $f(\mathbf{s},\mathbf{s}')$ and the phase $p(\mathbf{s},\mathbf{s}')$ depend only on the difference between unit vectors $\mathbf{s}$ and $\mathbf{s}'$, and therefore, they are functions of θ the difference between the polar angles of these vectors: $f(\mathbf{s},\mathbf{s}')=f(\theta)$, $p(\mathbf{s},\mathbf{s}')=p(\theta)$.

One important property of the phase function, which will be implemented later on, can be made on the basis of the optical theorem (2.9) and definition of the phase function (2.3). In forward direction, the phase function $p(0)=\sigma_s^{-1}(\mathrm{Im}f(0))^2$ (since, for a large particle, $|\mathrm{Im}f(0)| >> |\mathrm{Re}f(0)|$) and, if the particle is non-absorbing, the cross section $\sigma_s \approx 4\pi k^{-1}\mathrm{Im}f(0)$, therefore the phase function is proportional to the cross section: $p(0)=k^2/(4\pi)^2\sigma_s$. We note that

the phase function in forward direction has a wavelength dependent oscillatory component in phase to that of the cross section.

For small scattering angles θ, the phase difference between the rays scattered by different parts of the particle (see Fig. 2.4), is [11]

$$\delta = -\frac{kl}{2}\sin\theta\sin\gamma\cos\varphi, \tag{2.22}$$

where φ is the azimuthal angle of a vector oriented toward an element of the surface of the particle. Therefore, the scattering amplitude

$$f(\theta) \approx \frac{k}{2\pi i}\int dS\left(1 - e^{2ix(n_2-n_1)\cos\gamma}\right)e^{-ix\sin\theta\sin\gamma\cos\varphi} \tag{2.23}$$

where $dS = \sin\gamma\cos\gamma d\varphi d\gamma$. The φ integral can be taken immediately,

$$\int_0^{2\pi} d\varphi e^{ix\sin\theta\sin\gamma\cos\varphi} = 2\pi J_0(x\sin\theta\sin\gamma) \tag{2.24}$$

and, making the approximation $\sin\theta=\theta$, (2.19), becomes

$$f(\theta) \approx i\frac{xl}{2}\int_0^{\pi/2} d\gamma \sin\gamma\cos\gamma\left(1 - e^{2i\zeta\cos\gamma}\right)J_0(x\theta\sin\gamma), \tag{2.25}$$

with $\zeta=x(n_2-n_1)$. This result was first obtained by Van de Hulst [9]. The integral in (2.25) cannot be evaluated analytically and must be estimated.

Since the phase function is defined as

$$p(\theta) = \sigma_s^{-1}|f(\theta)|^2 = \sigma_s^{-1}\left((\mathrm{Re}\, f(\theta))^2 + (\mathrm{Im}\, f(\theta))^2\right), \tag{2.26}$$

the real and imaginary parts of the integral in (2.25) must be integrated separately. We then obtain the phase function in the small angle scattering approximation:

$$p_f(\theta) = \frac{l^2}{4\sigma_s}\left\{x^2\left(\frac{J_1(x\theta)}{x\theta} - \sqrt{\frac{\pi}{2}}\frac{J_{1/2}(y(\theta))}{\sqrt{y(\theta)}}\right)^2 + \right. \tag{2.27}$$

$$\left.\left(\frac{2(n_2-n_1)}{\theta^2 + 4(n_2-n_1)^2}\right)^2\left(\cos y(\theta) - \frac{\sin y(\theta)}{y(\theta)}\right)^2\right\},$$

where we have introduced the function

$$y(\theta) = x\sqrt{\theta^2 + 4(n_2-n_1)^2}\,. \tag{2.28}$$

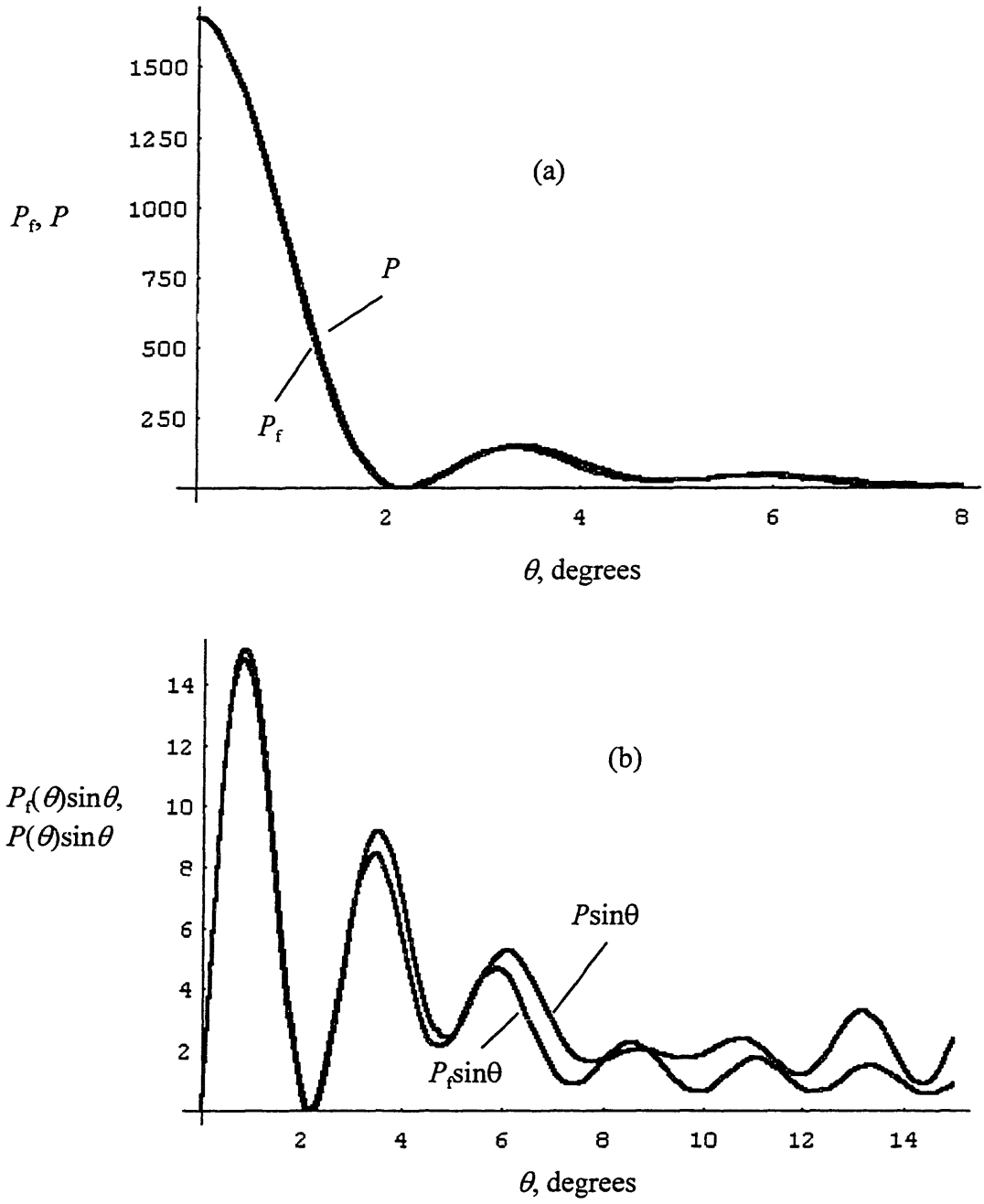

Figure 2.5 (a) - Comparison of phase function calculated in the Van de Hulst approximation, p_f, and that calculated using Mie theory, p. The functions are almost indistinguishable for small angles. (b) – Comparison of the phase functions multiplied by $\sin\theta$ (note that $\int p(\theta)\sin\theta d\theta = 1$).

The first term in (2.22) is obtained from the real part of the scattering amplitude, and the second term from the imaginary part. The phase function (2.27) can be used to describe the forward scattering of a large particle.

Just as with the cross section, the phase function depends on the size of the particle, its relative refractive index, and the wavelength of the incident light. This dependence is more complicated in the case of the phase function. The ratio $\frac{\sigma_s}{l^2}$ depends only on ρ. The ratio $\frac{p_f(\theta)}{x^2}$ depends on ζ and $x\theta$: $\sigma_s = \sigma_s(l,\rho)$ and $p_f(\theta) = p_f(x,\rho;\theta)$. We further note that the phase function does not depend on the absolute value of the particle size. The scattering curves for different values $(n_2\text{-}n_2)$ and l look the same in shape and differ only in scale.

The fact that the scattering amplitude in the forward direction is proportional to the cross section can be derived directly from (2.27). Indeed,

$$y(0)=2\zeta,\ \sqrt{\frac{\pi}{2}}\frac{J_{1/2}(2\varsigma)}{\sqrt{2\varsigma}} \approx \frac{\sin 2\varsigma}{2\varsigma},$$

the expression in brackets in (2.27) equals

$$\frac{x^2}{4}\left(1-\frac{\sin 2\varsigma}{\varsigma}+\frac{\sin^2\varsigma}{\varsigma^2}\right)^2,$$

and the phase function $p(0)\approx k^2/(4\pi)^2\sigma_s$. Thus, the phase function in the forward direction has an oscillatory component that is in phase to that of the cross section (2.12):

$$p_f(0) \approx \frac{x^2}{8\pi}\left(1-\frac{\sin\left(2x(n_2-n_2)\right)}{x(n_2-n_2)}+\left(\frac{\sin\left(x(n_2-n_2)\right)}{x(n_2-n_2)}\right)^2\right). \qquad (2.27a)$$

This conclusion will have a crucial impact on the results of section 2.2.

To test the validity of the approximate phase function (2.27) we can evaluate it in the Fraunhofer diffraction limit when $\rho>>1$ and $(n_2\text{-}n_2)<<1$:

$$p_f(\theta) = \frac{l^2}{4\sigma_s}\frac{J_1^{\,2}(x\theta)}{\theta^2}, \qquad (2.29)$$

which is a correct Fraunhofer diffraction phase function [12].

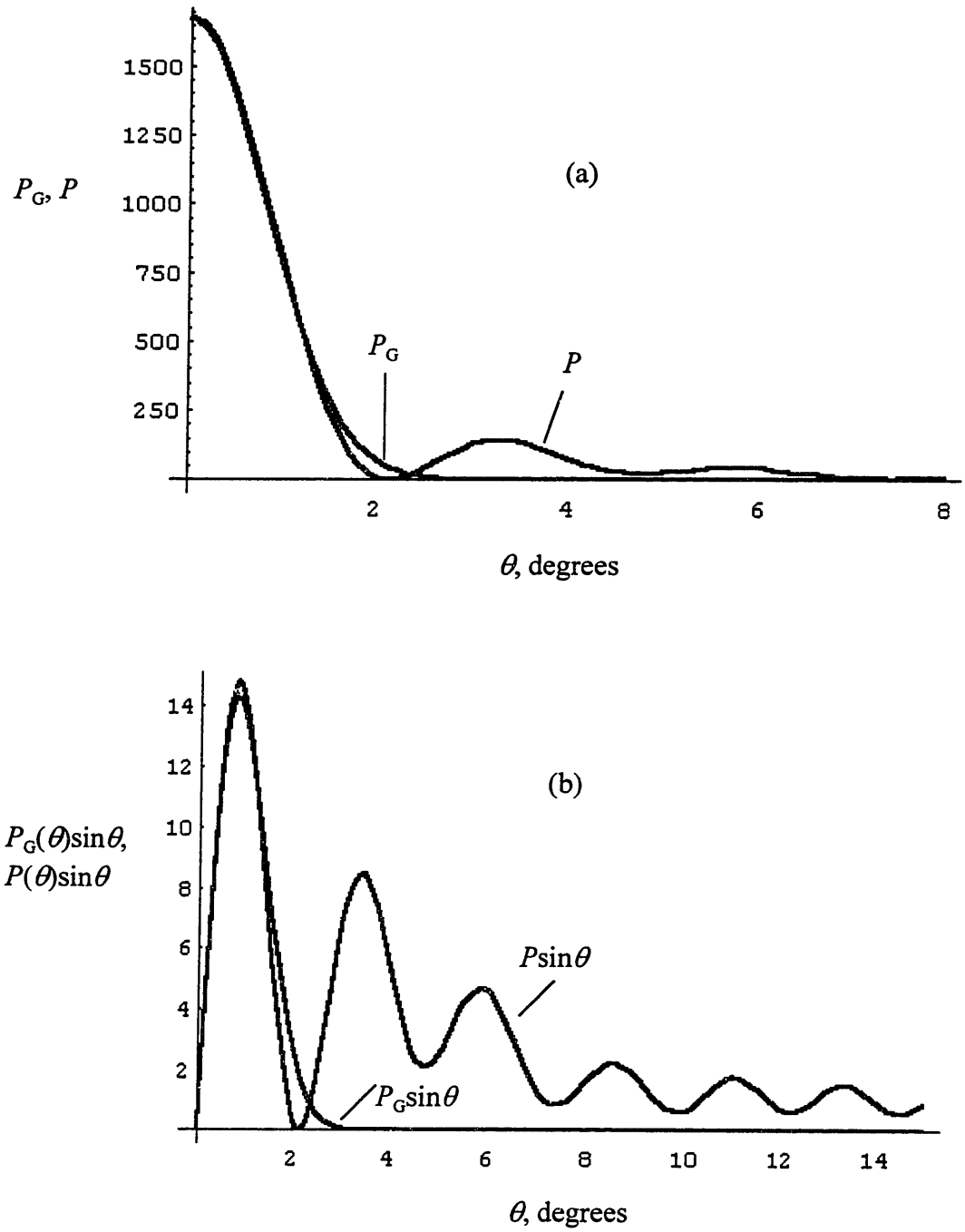

Figure 2.6 (a) -- Comparison of the Gaussian phase function, p_G, and the phase function calculated using Mie theory, p. The Gaussian phase functions approximates accurately only the first forward peak at angles θ<1.5°; (b) – Comparison of the phase functions multiplied by $\sin\theta$.

Let us go back to general expression (2.27), derived for small angle scattering. What is the angle range for which we can use it? Comparison of $p_f(\theta)$ with the phase function calculated in Mie theory, $p(\theta)$, shows that $p_f(\theta)$ describes $p(\theta)$ accurately for angles such that $x\theta \leq 20$; in other words , it is not valid when the number of maxima and minima of the Bessel's functions in (2.27) (and consequently the number of the maxima in the phase function) is much larger that unity. This illustrated in Fig. 2.5.

To describe small angle scattering, another approximate phase function is frequently used [1]. This is so called Gaussian phase function:

$$p_G(\theta) = 4\alpha W e^{-\alpha\theta^2}, \tag{2.30}$$

where α is proportional to $\theta_f^{-2} \approx \left(\frac{l}{\lambda}\right)^2$ and W is a normalization parameter. W should be chosen either to satisfy the normalization rule for the phase function or to better approximate its behavior in some angle interval. The Guassian phase function is simpler than $p_f(\theta)$. The main disadvantage of using $p_G(\theta)$ is that it accurately approximates the Mie phase function only for such angles θ that $x\theta \leq 2$. (Roughly speaking, it is 10 times worse than $p_f(\theta)$.) It describes well only the forward peak (Fig.2.6). In some cases this can be sufficient, since, for example, the forward peak of a particle with $l/\lambda \approx 10$ and a small refractive index ($n_2/n_1 - 1 \approx 0.1$) contains approximately 70% of the scattering power. However, as discussed below, it can not describe some important effects. In this case, a modified Gaussian phase function (2.78, below) can be used.

2.1.2.2 Backscattering

In this section we estimate the phase function for scattering angles near the backward direction. We obtained the phase function in the small angle scattering approximation. This approximation, however, is not valid for non-forward scattering, particularly backscattering. To find the phase function for angles θ close to π we need to use Mie theory. We surely can estimate numerically the phase function for these angle values. However, some important

properties can be obtained without the use of rigorous numerical computations. Let us first speculate on what kind of scattering we should expect in the backward direction.

One can predict that backscattering is negligible if the scatterer is large. At the same time, we know from the scattering theory that [10]

$$|f(\theta)| = \frac{1}{\sin\theta}\frac{b}{|d\chi/db|} \tag{2.31}$$

with b an impact parameter and χ the corresponding deflection angle (Fig.2.7). This would suggests that the cross section in the backward direction is infinite, if backscattering is possible for impact parameters other than zero. In fact, strong backscattering is a striking phenomenon observed when sunlight is scattered from clouds, called the glory. In the WKB approximation [9]

$$|f(\theta')|^2 = \frac{b_g}{\lambda\left|d\chi/db\right|^2\Big|_{b=b_g}}\left(J_0(kb_g\sin\theta')\right)^2. \tag{2.32}$$

In this expression θ is the scattering angle measured from the backward direction, b_g is the impact parameter that leads to exact backward scattering, and the derivative in the denominator is evaluated at this point. The phase amplitude is not zero in the backward direction if there is an impact parameter $b_g \neq 0$. This is possible if a multiple reflections inside the particle can lead to an outgoing beam in the exact backward direction. Examples of such paths are shown in Fig. 2.8. It may appear that a non-zero b_g exists for any spherical particle. This is not entirely true. The particle must be large enough to permit such trajectories. That is why the presence of a scattering peak in the backward direction is a property of large particles only. The refractive index may limit number of permissible inner reflections. For example, the double reflectance path (a) in Fig. 2.8 is possible only if the relative refractive index of the particle $n=n_2/n_1$ is higher than $\sqrt{3}$ and less than 2. The glory observed during illumination of such particle would be very strong. Triple reflectance (path (b) on Fig. 2.8) results in a weaker effect, but is possible for smaller n. The trajectories of higher orders are possible as well. In general, the more reflections necessary, the smaller the backscattering amplitude and bigger b_g.

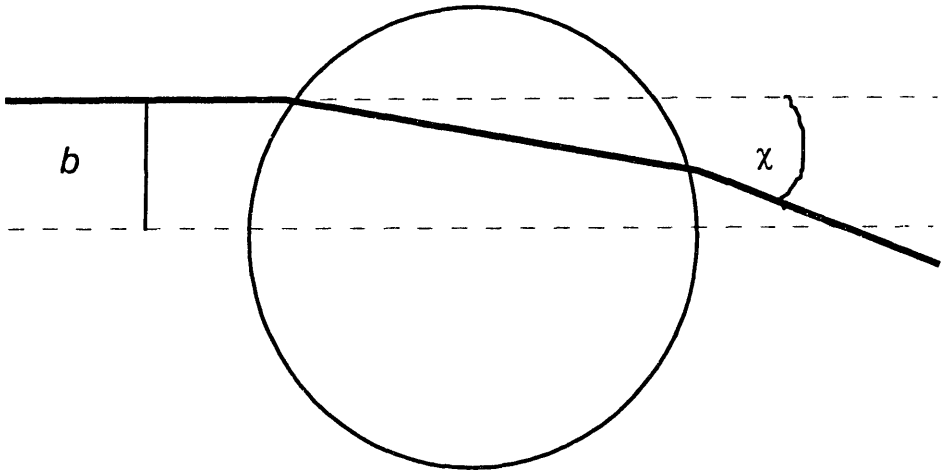

Figure 2.7 Impact parameter b and deflection angle χ

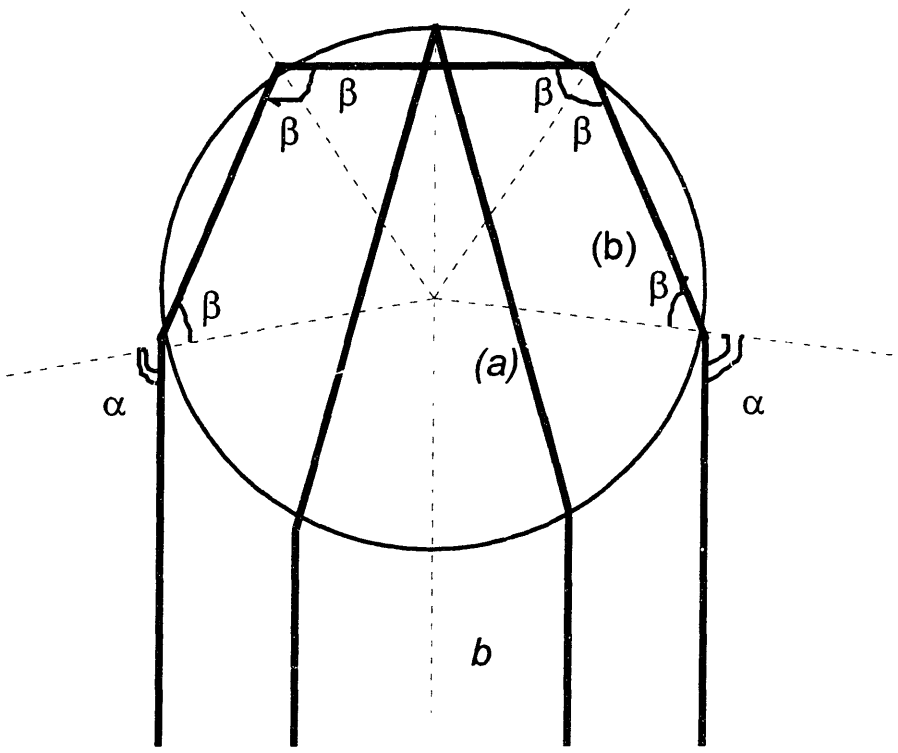

Figure 2.8 Examples of the possible trajectories of photons inside the particle that result in exact backward scattering for impact parameter $b \neq 0$. (a) – double trajectory; (b) – triple trajectory.

Our goal now is to evaluate the phase function in the backward direction. Substituting (2.32) into (2.3) we obtain

$$p(\theta') = \frac{b_g}{\lambda \left| d\chi/db \right|^2 \Big|_{b=b_g} \sigma_s} \left(J_0(lb_g \sin\theta') \right)^2 . \tag{2.32a}$$

Now we need to estimate b_g and $d\chi/db$. For a trajectory with k internal reflections, the deflection angle equals

$$\chi = 2\alpha - 2(k+1)\beta + k\pi \tag{2.33}$$

with α the angle of incidence, and β the angle of refraction. In exact backward direction, $\chi = 2\pi$ and angle β can be expressed as

$$\beta = \frac{(k-2)\pi + 2\alpha}{2(k+1)} . \tag{2.33a}$$

Substituting (2.33a) into the relationship between the angle of incidence and angle of refraction $\sin\alpha = n\sin\beta$ we obtain a transcendental equation

$$\sin\alpha = n \sin\left(\frac{(k-2)\pi + 2\alpha}{2(k+1)} \right) \tag{2.33b}$$

which should be numerically solved for α. Then, the impact parameter can be found as well: $b_g = (l/2)\sin\alpha$. The derivative $d\chi/db$ can be obtained from (2.33):

$$d\chi = 2d\alpha - 2(k+1)d\beta . \tag{2.33c}$$

Substituting $d\alpha = \frac{\partial\alpha}{\partial b} db$, $d\beta = \frac{\partial\beta}{\partial\alpha}\frac{\partial\alpha}{\partial b} db$ into (2.33c) we obtain

$$\frac{d\chi}{db} = 2\frac{\partial\alpha}{\partial b}\left(1 - (k+1)\frac{\partial\beta}{\partial\alpha} \right) . \tag{2.33d}$$

From the relationship $b_g = (l/2)\sin\alpha$ one can find $\frac{\partial\alpha}{\partial b} = \frac{2}{l\sqrt{1 - 2b^2/l^2}}$, and from the equation $\sin\alpha = n\sin\beta$ one can find $\frac{\partial\beta}{\partial\alpha} = \frac{\sqrt{1 - 2b^2/l^2}}{\sqrt{n^2 - 2b^2/l^2}}$. After substitution these derivatives into (2.33d), we obtain

$$\left|\frac{\partial\chi}{\partial b}\right|^2 = \frac{8}{l^2\left(n^2-1\right)^2}, \tag{2.33e}$$

Substituting (2.33e) into (2,32), one can determine the phase function for backward scattering:

$$p(\theta) \approx \frac{xl^2}{16\pi\sigma_s}\left(n^2-1\right)^2\left(J_0(x\theta)\right)^2, \tag{2.34}$$

where we approximated $\sin\theta\approx\theta$. This expression will be used in section 2.2.1.

This simple expression, obtained without employing rigorous and complicated Mie theory, shows a number of important properties of the backscattering.

(1) The larger the particle, the stronger the backscattering. It reaches a maximum when $\theta=\pi$. For a large particle ($\zeta>>1$), this maximum can be obtained from (2.34):

$$p(\pi) \approx \frac{x}{8\pi^2}\left(n^2-1\right)^2\left\{1+\frac{\sin\left(2x(n_2-n_1)\right)}{x(n_2-n_1)}-\left(\frac{\sin\left(x(n_2-n_1)\right)}{x(n_2-n_1)}\right)^2\right\}. \tag{2.35}$$

As can be seen, the maximal value of the phase function is linearly proportional to $x=\pi l/\lambda$.

(2) The angular oscillations are determined by the Bessel function in (2.34), which depends on the argument $x\theta$. Thus, the larger the particle, the more rapid the angular oscillations and the smaller the width of the backward peak. Simply speaking, the larger the particle, the sharper the peak.

(3) Expression (2.35) shows that the amplitude of the backscattered light exhibits a functional dependence on wavelength. In contrast to the forward scattering phase function (compare $p(\pi)$ given by (2.35) with $p(0)$ given by (2.27a)) which, as a function of λ, oscillates in phase with the cross section, the backscattering oscillations are shifted by half a period. Thus, when the forward scattering and the cross section have maxima, the backscattering has minima. The fact that the forward scattering and the cross section are in phase is a direct result of the optical theorem. The behavior of the backscattering can be explained by the fact that a scattered light from a large particle is either predominantly forward or backward directed. The scattering for intermediate angles is very weak.

Because of the quasiclassical approximation used to derive the backscattering phase function, it is slightly different from that predicted by the Mie theory. In reality, the backscattering peak is reached not in the exact backward direction but slightly shifted

(Fig.2.9). This shift depends only on the parameter x and equals $\Delta\theta=\pi/x$. (To correct the description of this shift to expression (2.34), one needs to substitute the argument, θ, of the Bessel function in (2.24) with $\theta-\Delta\theta$). The shift does not change any of the predictions made regarding the backscattering.

One important property of the backscattering should be emphasized. While the backward peak is significantly smaller than that for forward scattering, it can be comparable or even larger than the light intensity that would be scattered in the same direction by an "isotropic scatterer" (in which scattering is the same in all angles). A particle with diameter l=10μm and n=1.1 has a maximum value of the backward peak for λ=0.4μm of approximately p_{max}=0.12. The power flux collected in a small solid angle $d\Omega$ around the backward direction will be

$$I_\Omega = p_{max}\, d\Omega \tag{2.36}$$

and $I_\Omega/d\Omega$=0.12. For comparison, an isotropic scatterer irradiates $p(\theta)=1/(4\pi)$ in all directions including the backward one, and $\frac{I_\Omega}{d\Omega}=\frac{1}{4\pi}\approx 0.08$, one and a half times less than that of the 10μm particle.

In conclusion, let us discuss briefly how the scattering pattern changes with particle size. When the scatterer is smaller than the wavelength ($x<<1$), scattering is described by the Rayleigh or Rayleigh-Gans theory. The efficiency parameter (the cross section divided by the cross sectional area of the particle) is proportional to x^4 and the cross section has the famous λ^{-4} wavelength dependence. This type of scattering is responsible for the blue color of the sky and for the effectiveness of yellow illumination lamps in hazy morning weather. As the particle size increases, the scattering becomes less isotropic and more forward directed. The scattering is strongest when the particle has a diameter close to the wavelength (l=0.1--1μm). The angular distribution of the scattered light exhibits a prominent forward-directed peak. The width of this peak decreases with increasing particle size. The phase function decreases almost monotonically with angle θ. Backscattering is negligible. This type of scattering is responsible for light diffusion in biological materials. With further increase in size, scattering at angles near $\theta=\pi/2$ diminishes and a backward-directed peak is formed. For particles larger than the

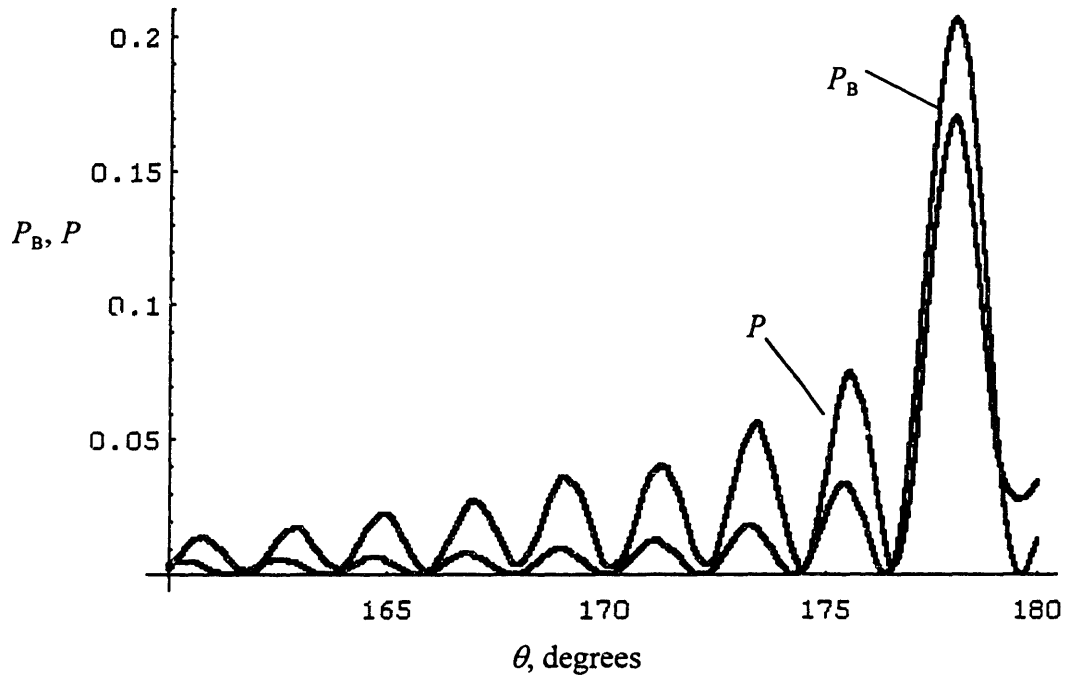

Figure 2.9 Comparison of the phase function calculated in the WKB approximation for scattering in backward directions, p_B, and the phase function calculated using Mie theory (l=10μm, λ=0.5μm n=1.08). The phase functions plotted here are already integrated over the phase angle φ.

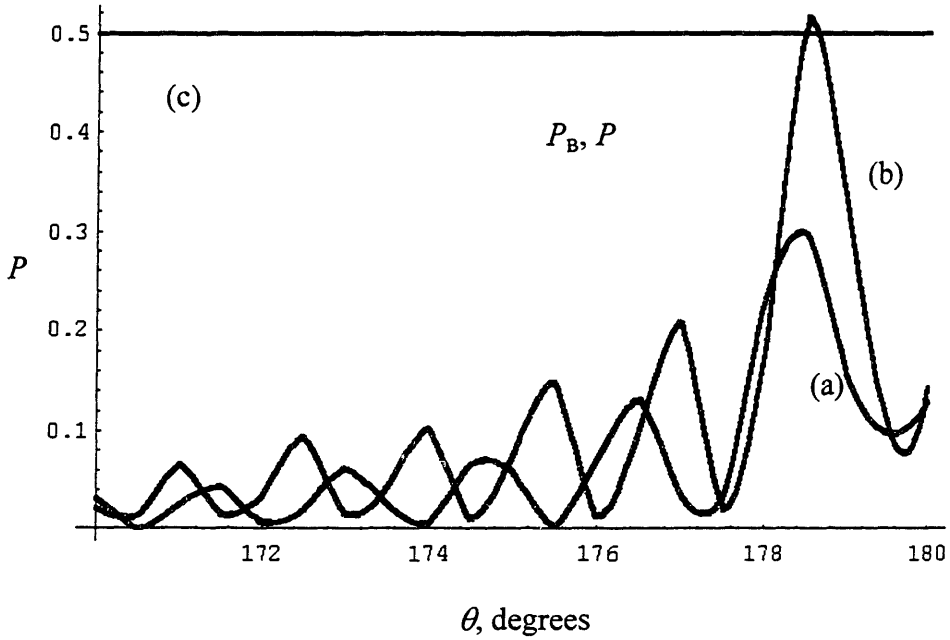

Figure 2.10 Comparison of the backscattering peak for a sphere (l=10μm) with scattering from an "isotropic scatterer" for two different wavelengths: (a) -- λ=400nm; (b) -- λ=350nm; (c) – "isotropic scatterer".

wavelength (l=5--20μm), scattering is characterized by a very strong forward peak, noticeable backscattering, and very weak scattering in lateral directions. The efficiency parameter is no longer proportional to x, and exhibits oscillations around the value 2. This type of scattering is responsible for such illustrious effects as the rainbow, the glory, and the ineffectiveness of yellow street light illumination in a real London fog. Despite these well known effects, large particle scattering has being disregarded in biological spectroscopy. This is partly due to the fact that light inside the tissue is randomized by multiple scattering from smaller structures of size comparable to the wavelength (extracellular matrix, cellular organelles such as mitochondria, etc.). However, the light is not randomized in the uppermost layer of the tissue. Thus, if this layer contains some structures with dimensions larger than the wavelength, the pattern of the light scattered by these structures can manifest itself.

2.1.3 Important results from this section

In this section the light scattering by a single particle large relative to the wavelength was studied. In section 2.1.1 the optical cross section of a large particle (2.12) was derived in the Van de Hulst approximation [11]. This cross section depends on the size of the scatterer, the wavelength, and the difference in refractive indexes between the scatterer and the surrounding medium. The cross section has an oscillatory wavelength dependence with the periodicity proportional to the particle diameter.

In section 2.1.2 the phase function of a large scatterer is discussed. Since large particles scatter light predominantly in forward and backward directions, these two cases were considered. The phase function for near forward scattering (2.27) was derived in the Van de Hulst approximation (section 2.1.2.1). It was shown that its amplitude has an oscillatory component (2.27a) that is in phase to that of the cross section, as required by the optical theorem. The phase function for near backward scattering (2.34) was derived in section (2.1.2.2). Its amplitude in exact backward direction (2.35) has the oscillatory component which is out of phase to the oscillations of the cross section.

In the following section we will use these results to study light reflectance from a slab of large particles. It will be shown that the wavelength dependent oscillations of the cross section give rise to an oscillatory component in the reflectance from the slab.

2.2 Reflectance from a slab of large particles

Mucosal tissues, which line the hollow organs of the body, generally consist of a surface layer of epithelial cells supported by underlying, relatively acellular connective tissue. In healthy tissues the epithelium may consist of a single, well-organized layer of cells typically 10-20 μm in diameter. In cancerous and pre-cancerous (dysplastic) epithelium the cells proliferate, the cellular layer often thickens and becomes more tightly packed, and the cell nuclei become enlarged [8]. The cell nuclei in the epithelial layer are spheroidal scatterers with refractive index higher than that of the surrounding cytoplasm [6,7]. In healthy epithelium, the nuclei range in size from 4 μm to 7 μm. In contrast, dysplastic nuclei can have diameters as large as 20 μm, occupying almost the entire cell volume. Thus, in the visible range, the wavelength $\lambda << l$, and the Van de Hulst approximation can be used to describe the optical scattering cross section and the phase function of these nuclei. Therefore, their scattering cross section exhibits oscillations in wavelength described by expression (2.12).

When a biological tissue is irradiated by light, fraction of light is reflected from the tissue surface (specular reflectance), the remaining light penetrates into the tissue and, if not absorbed, eventually returns back and partially collected. The ratio of this signal to that of the incident light is called reflectance signal. It will be shown that the wavelength dependent oscillations of the cross section give rise to a corresponding oscillatory component in the reflectance from the tissue.

Consider a beam of light incident on the surface of epithelial tissue. A portion of this light will be backscattered from the epithelial nuclei, while the remainder will be transmitted to deeper tissue layers, where it undergoes multiple scattering and becomes randomized. All of this "diffusive" light which is not absorbed in the tissue eventually returns to the surface,

passing once more through the epithelium, where it is again subject to scattering from the cell nuclei. Thus, the emerging light will consist of a large diffusive background plus the component of forward scattered and backscattered light from the nuclei in the epithelial layer. The contributions of the backscattered and the forward scattered light are independent and will be studied separately in sections 2.2.1 and 2.2.2 respectively.

2.2.1 Backscattering from a slab of large particles (cell nuclei)

Consider a plane wave propagating in direction $\mathbf{s}_i$ close to the normal to the surface (axis **z**) of a slab of thickness L containing randomly distributed scattering particles (cell nuclei) with the size distribution $N(l)$ (the number of particles per unit area and per unit interval of diameters). We consider here only photons that are scattered once by the particles in the near-backward direction (Fig. 2.11, path (1)). We do not consider photons scattered more than once in the epithelial layer (path (2) in Fig. 2.11) nor photons which are transmitted to the underlying tissue layers and then return back (path (3) in Fig.2.11). Contributions of these photons to the oscillatory fine structure will be considered in the next section). Thus, backscattering from a slab is essentially a single elastic scattering process, although the slab may contain many scatterers.

Consider light incident into the slab in direction **s** and specific intensity $I_i(\mathbf{s})$ [1] (unit $\mathrm{mWsr^{-1}mm^{-2}Hz^{-1}}$). Each particle of a diameter l scatters the power $\sigma_s(l)I_i$, where $\sigma_s(l)$ is the scattering cross section of such particle. Therefore, the decrease of the specific intensity $dI(\mathbf{r},\mathbf{s})$ on the distance dr due to the scattering from the particles with diameters from l to $l+dl$ is expressed by

$$dI(\mathbf{r},\mathbf{s})=-\eta(\mathbf{r},l)\,\sigma_s(l)I(\mathbf{r},\mathbf{s})drdl,$$

with $\eta(\mathbf{r},l)$ the size distribution of the number density (the number density [1] $\rho(\mathbf{r})=\int \eta(\mathbf{r},l)dl$). In the case of the homogenous spatial distribution of the scatterers the decrease of the specific intensity due to the scattering from all the particles inside the slab

$$dI(\mathbf{r},\mathbf{s})=-\int\eta(l)\,\sigma_s(l)dl\,I(\mathbf{r},\mathbf{s})dr.$$

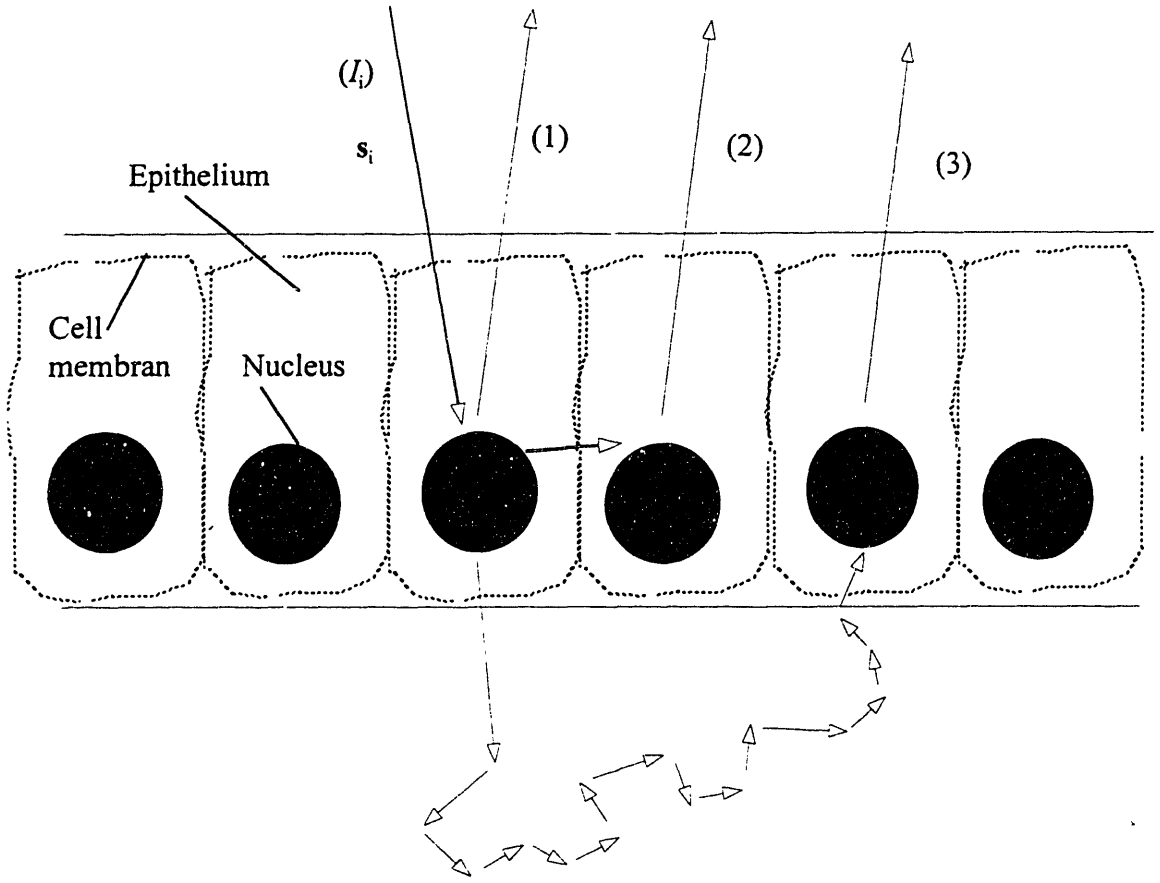

Figure 2.11. Possible photon paths in reflected light. (I_i)- initial light, (1) - photons reflected after one backscattering event, (2) - photons backscattered after a number of scattering events inside epithelium, (3) - photons diffusely reflected from underlying layers.

Since $dz=\cos\theta dr$ with θ the angle between the direction **s** and the normal to the surface directed toward the slab, and, because of the spatial homogeneity, $N(l)= \eta(l)L$, the specific intensity of light that propagates through this slab in direction **s** without being scattered can be expressed as

$$I(\mathrm{s}) = \exp\left(-\frac{\tau}{\cos\theta}\right) I_i(\mathrm{s}),$$

where τ is called the optical distance:

$$\tau = \int \sigma_s(l) N(l) dl . \tag{2.37}$$

Therefore, the probability of a photon to propagate through the slab without being scattered equals $\exp\left(-\frac{\tau}{\cos\theta}\right)$ and the probability of a photon to be scattered inside the slab is

$$1-\exp\left(-\frac{\tau}{\cos\theta}\right).$$

The phase function $p(\mathbf{s},\mathbf{s}')$ is equal to the probability of a photon being scattered from its initial direction $\mathbf{s}$ to direction $\mathbf{s}'$ given that the scattering event takes place. Thus, the probability of a photon to be backscattered in direction $-\mathbf{s}'$ inside the slab is

$$\left(1-e^{-\frac{\tau}{\cos\theta}}\right)p(\mathbf{s},-\mathbf{s}'), \tag{2.37a}$$

where the negative sign before $\mathbf{s}'$ indicates that the scattering is in the backward direction, and $p(\mathbf{s},-\mathbf{s}')$ is the effective phase function which is the weighted average of $p(l,\mathbf{s},\mathbf{s}')$ over scatterers of all sizes:

$$p(\mathbf{s},\mathbf{s}') = \frac{1}{\tau}\int p(l,\mathbf{s},\mathbf{s}')\sigma_s(l)N(l)dl , \tag{2.38}$$

with $p(l,\mathbf{s},\mathbf{s}')$ the phase functions of a particle with diameter l.

Thus, the backscattered intensity flux collected in solid angle Ω_c is

$$I_b = \int_{\Omega_c}\int_{\Omega_i} I_i(\mathbf{s})p(\mathbf{s},-\mathbf{s}')\left(1-e^{-\frac{\tau}{\cos\theta}}\right)ds\,ds' , \tag{2.39}$$

where $I_i(\mathbf{s})$ is the specific intensity of the incident light delivered in solid angle Ω_i. We will refer to this expression in section 2.3.

To appreciate the physical meaning of expression (2.39), let us consider an important case of a small optical distance τ and small angles Ω_c and Ω_i. This approximation holds in many practical applications, including our experiments with tissue phantoms and esophageal tissues discussed in chapter 3 (in our case $\Omega_c=\Omega_i=0.15$). In this case, expending (2.39) to first order in τ and $1-\cos\theta$ (small Ω_i approximation) and substituting (2.34) into (2.39), one can obtain the reflectance associated with the backscattering

$$R_b(\lambda) \equiv \frac{I_b(\lambda)}{I_i} \approx \frac{x}{16\pi}\left(n^2-1\right)^2 \int l^2 N(l)dl\left(1-\tfrac{1}{2}\int N(l)\sigma_s(\lambda,l)dl\right). \tag{2.40}$$

Note that the send term in the brackets is proportional to τ. Thus, the reflectance as a function of wavelength consists of a constant "background" proportional to the relative surface area covered by the scatterers,

$$\int l^2 N(l)dl, \tag{2.41}$$

plus an oscillatory component proportional to $-\tau$ which is out of phase with the cross section (2.12). The cross section (2.12) contains two wavelength dependent terms, one is proportional to ζ^{-1} and the second is proportional to ζ^{-2}. Noticing that in our case, $\zeta>>1$ and the second term, proportional to ζ^{-2}, can be neglected, the wavelength dependence of this oscillatory component is approximated by

$$\int \frac{\sin\left(\frac{2\pi l}{\lambda}(n_2-n_1)\right)}{\frac{\pi l}{\lambda}(n_2-n_1)} N(l)\frac{\pi l^2}{4}dl, \tag{2.42}$$

As can be seen, particles of each diameter contribute

$$\frac{\sin\left(\frac{2\pi l}{\lambda}(n_2-n_1)\right)}{\frac{\pi l}{\lambda}(n_2-n_1)} \tag{2.43}$$

to the reflectance signal. Each contribution is proportional to the factor

$$N(l)\frac{\pi l^2}{4}dl, \tag{2.44}$$

which is the ratio of the total cross sectional area of all the particles of this particular size to the total area of the surface. In the case of an epithelial tissue consisting of one cell layer, this factor is called the nucleus-cytoplasm ratio (N/C-ratio). These observed oscillations can be analyzed by solving the "inverse problem" to determine the size distribution, $N(l)$ (see section 2.3).

2.2.2 Light propagation through a slab of large particles

In the previous section we considered the backscattering from a slab of large particles. Since the backscattering is much smaller than the scattering in forward directions, the main portion of the incident light penetrates through epithelium into deeper tissue layers (connective tissue of lamina propria and musclular tissue of muscularis mucosa). The connective tissue layer is relatively acellular and is usually thicker and more homogenous than the epithelium [14]. Many investigators have established that the photons are randomized there, and that light propagation is governed by diffusion [15]. Some photons are absorbed and the rest are scattered back toward the surface. Such photons pass through the epithelium, where they are scattered from the cell nuclei. If the optical distance of the epithelium $\tau \leq 1$, the probability of multiple scattering is small. In that case, the first order multiple scattering approximation is applicable. This is the relevant case when we consider simple columnar one-cell-layer epithelium that covers most of the surface of the gastrointestinal tract, respiratory system, etc. This case will be considered in section 2.2.2.1, and will be applied in Chapter 3 to analyze the experimental results. If, however, the optical distance is no longer small, multiple scattering can not be ignored and the transport equation must be solved. An approximate solution valid in this regime is obtained in section 2.2.2.2. This situation is less frequent for epithelial tissues. An example is a thick stratified epithelium of the skin (epidermis). If $\tau >> 1$, the diffusion approximation [1] gives relatively simple solutions, and the transport equation need not be solved. This regime is almost never achieved in surface epithelium and is not considered here.

2.2.2.1 Small optical distance - first order multiple scattering approximation

Consider light with angular dependence $I_d(\theta')$ which is incident on the slab from below, with angle θ being measured from the normal to the surface directed toward the slab (Fig. 2.12). Note that I_d is the diffuse specific intensity, not the incident specific intensity, I_i. Diffuse photons come from deeper tissue layers and their angular distribution is broad, in contrast to that of the incident light which can be confined by the delivery optics to a small solid angle. We collect light emerging from the slab in some solid angle Ω_C. Two types of photons can be collected in a direction θ. Some photons propagate through the slab without being scattered (path (1) of Fig. 2.12). Since the probability of a photon to propagate through the slab without being scattered equals $\exp\left(-\frac{\tau}{\cos\theta}\right)$ (see section 2.2.1), the specific intensity from these photons is

$$I_d(\theta)e^{-\frac{\tau}{\cos\theta}}. \tag{2.45}$$

the remaining photons undergo scattering inside the slab. If $\tau \leq 1$, we can neglect the scattering of the photons that have been scattered once. The probability that a photon passes distance r without being scattered is $e^{-\tau(r)}$ with $\tau(r)$ the *optical* distance corresponding to the distance r:

$$\tau(r) = \int_0^r dr' \int dl \eta(r', l)\sigma_s(l). \tag{2.46}$$

If the spatial distribution of the scatterers in the slab is uniform, the optical distance is proportional to z:

$$\tau(r) = \frac{z\chi}{\cos\theta'},$$

where we introduced the factor

$$\chi = \int dl \eta(l)\sigma_s(l) \tag{2.47}$$

and we used the fact that $dz = \cos\theta\, dr$. Therefore, the specific intensity of light propagating this distance without being scattered is

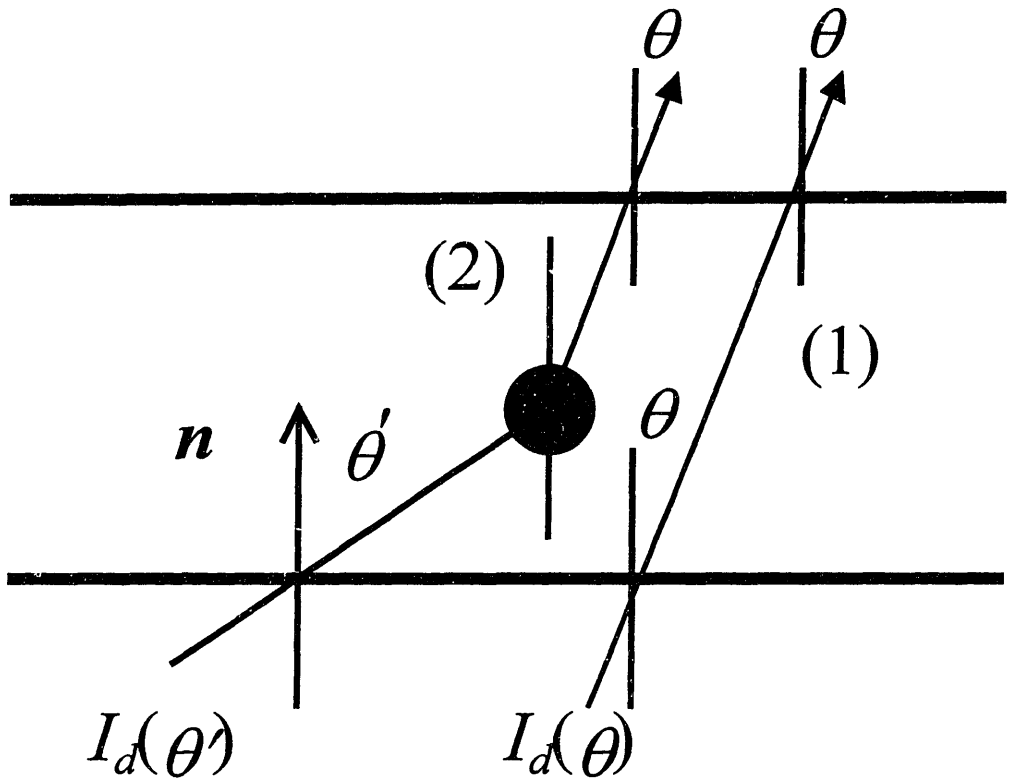

Figure 2.12. Possible paths of the photons collected after transmission through the slab in a direction with phase angle θ. A photon can come out in this direction without scattering (path 1) or after being scattered once (path 2).

$$I_d(\theta')\exp\left(-\frac{z\chi}{\cos\theta'}\right). \tag{2.48}$$

The probability of a photon to be scattered between point z and $z+dz$ equals

$$\frac{z\chi}{\cos\theta'}dz\,. \tag{2.49}$$

The probability of a photon to be scattered to the direction **s** determined by polar angle θ' equals

$$p(\mathbf{s},\mathbf{s}')\frac{z\chi}{\cos\theta'}dz\,. \tag{2.50}$$

The specific intensity scattered to this direction is

$$I_d(\theta')p(\mathbf{s},\mathbf{s}')\frac{z\chi}{\cos\theta'}\exp\left(-\frac{z\chi}{\cos\theta'}\right)dz. \qquad (2.51)$$

The contribution to the specific intensity of the exiting light at angle θ from photons which enter the slab at angle θ' is obtained integrating (2.51) over penetration depth z:

$$I_d(\theta')p(\mathbf{s},\mathbf{s}')\int_0^L \frac{e^{-\frac{z\chi(z)}{\cos\theta'}}}{\cos\theta'}\chi dz, \qquad (2.52)$$

where L is the thickness of the slab.

The contribution of the photons coming from all incident angles is

$$2\pi\int_0^{2\pi}\sin\theta' d\theta'\frac{I_d(\theta')p(\theta,\theta')}{\cos\theta'}\int_0^L e^{-\frac{z\chi}{\cos\theta'}}\chi dz, \qquad (2.53)$$

where we have written the phase function p as a function of polar angles θ and θ′ to simplify the following expressions (the phase function of a spherical particle does not depend on the azimythal angles and depends on the difference θ-θ′).

Incorporating (2.45) and (2.53), we obtain the transmitted intensity

$$I_f = 2\pi\int_0^{\theta_c} I_d(\theta)e^{-\frac{\tau}{\cos\theta}}\sin\theta d\theta + 2\pi\int_0^{\theta_c}\sin\theta d\theta\int_0^{2\pi}\sin\theta' d\theta'\frac{I_d(\theta')p(\theta,\theta')}{\cos\theta'}\int_0^L dz e^{-\frac{z\chi(z)}{\cos\theta'}}\chi, \qquad (2.54)$$

with θ_c the angular width of Ω_c. The integration over z can be performed and expression (2.54) reduces to

$$I_f = 2\pi\int_0^{\theta_c} I_d(\theta)e^{-\frac{\tau}{\cos\theta}}\sin\theta d\theta + 2\pi\int_0^{\theta_c}\sin\theta d\theta\int_0^{2\pi}\sin\theta' d\theta' I_d(\theta')p(\theta',\theta)\left(1-e^{-\frac{\tau}{\cos\theta'}}\right). \qquad (2.55)$$

To perform the integration in (2.55) we need to know angular dependence of $I_d(\theta)$. Diffusion theory predicts that the angular distribution of the reflected light has, to a very good, approximation, a $a+b\cos\theta$ dependence (see section 3.3) [17]. One can show that, in this case, expression (2.55) involves the integrals of the hypergeometric functions that allow only numerical evaluation.

In many important practical applications, angles Ω_c and Ω_i are small and $\tau\leq 1$ (see the discussion on the applicability of this approximation in section 2.2.1). The angular

dependence of the phase function in (2.55) is much stronger than that of $I_d(\theta)$ and $\cos\theta$ and we can then expend (2.55) in 1-cosθ<<1:

$$I_f = 2\pi e^{-\tau}\int_0^{\theta_c} I_d(\theta)\sin\theta d\theta + 2\pi\left(1-e^{-\tau}\right)\int_0^{\theta_c}\sin\theta' d\theta'\int_0^{2\pi}\sin\theta d\theta I_d(\theta)p(\theta,\theta') - \qquad (2.56)$$

$$-2\pi\tau\left\{e^{-\tau}\int_0^{\theta_c} I_d(\theta)(1-\cos\theta)\sin\theta d\theta + \left(1-e^{-\tau}\right)\int_0^{\theta_c}\sin\theta' d\theta'\int_0^{2\pi}\sin\theta d\theta I_d(\theta)p(\theta,\theta')(1-\cos\theta')\right\}$$

where we expended

$$e^{-\frac{\tau}{\cos\theta}} \approx e^{-\tau}\left(1-\tau(1-\cos\theta)\right).$$

The terms in figure brackets in (2.56) are much smaller than the first two terms and can be neglected:

$$I_f = 2\pi e^{-\tau}\int_0^{\theta_c} I_d(\theta)\sin\theta d\theta + 2\pi\left(1-e^{-\tau}\right)\int_0^{\theta_c}\sin\theta' d\theta'\int_0^{2\pi}\sin\theta d\theta I_d(\theta)p(\theta,\theta'). \qquad (2.56a)$$

We shall use this expression in section 2.3.

If the optical distance is small, as well, we can expend (2.56a) in τ:

$$I_f = 2\pi\int_0^{\theta_c} I_d(\theta)\sin\theta d\theta + 2\pi\tau\left\{\int_0^{\theta_c}\sin\theta' d\theta'\int_0^{2\pi}\sin\theta d\theta I_d(\theta)p(\theta,\theta') - \int_0^{\theta_c} I_d(\theta)\sin\theta d\theta\right\}. \qquad (2.57)$$

Let us define the normalized transmitted intensity

$$\bar{I}_f = \frac{I_f}{\langle I_d\rangle_{\Omega_c}},$$

where $\langle I_d\rangle_{\Omega_c}$ is the averaged diffuse intensity

$$\langle I_d\rangle_{\Omega_c} = 2\pi\int_0^{\theta_c} I_d(\theta)\sin\theta d\theta. \qquad (2.58)$$

Since the diffuse specific intensity changes slowly with angle, in the case of a small collection angle θ_c, $\bar{I}_f$ can be obtained from (2.57):

$$\bar{I}_f = 1-\tau\left\{1-\int_0^{\theta_c}\sin\theta d\theta\bar{I}_d(\theta)p(0,\theta)\right\}, \qquad (2.59)$$

where $\bar{I}_d(\theta)$ is the normalized diffuse intensity

$$\bar{I}_d(\theta) = \frac{I_d(\theta)}{\langle I_d \rangle_{\Omega_c}}.$$

Expression (2.58) shows that the transmitted light has a component which is proportional to -τ, just as in the case of backscattering (2.40). Thus, light backscattered from the particles inside the slab and diffusive light propagating through the slab introduce an oscillatory component which is proportional to -τ. Note that these two effects are additive.

2.2.2.2 Large optical distance - small angle approximation

Backscattering and forward scattering of diffuse light both exhibit an oscillatory component in the reflectance. Its amplitude is proportional to the concentration of the scatterers if the optical distance $\tau \leq 1$. In same rare cases the epithelium may be thick enough so that τ is no longer smaller than unity, but not large enough to result in complete diffusion. The goal of this section is to understand how the oscillatory component behaves for such τ. (The results presented here will not be used in the following sections.)

When $\tau \leq 1$ the first order or single scattering approximation can be used. When $\tau >> 1$, we are in the diffuse regime. In the intermediate case, we need to solve the equation of transfer [1]

$$\mathbf{s} \cdot gradI(\mathbf{r},\mathbf{s}) = -\mu_t I(\mathbf{r},\mathbf{s}) + \mu_t \int_{4\pi} I(\mathbf{r},\mathbf{s}')p(\mathbf{s}',\mathbf{s})ds' \qquad (2.61)$$

where $\mu_t = \rho\sigma_t$ is extinction coefficient, ρ is the number density [1]; as before, $I(\mathbf{r},\mathbf{s})$ is the specific intensity at point **r** in direction **s**. This equation states that the change of specific intensity in a given direction, **s**, equals the difference between the portion scattered to this direction from all other directions and the portion absorbed or scattered in all other directions from the given one. The transport equation describes not only light propagation in turbid media but also many other processes, such as propagation of acoustic waves, neutron transport, traffic in a city, and even money flow in a large corporation. The equation was first formulated by Schuster in 1902. Despite extensive studies, the transport equation has not being solved for an arbitrary phase function. Many attempts have been made to solve it, if not

in general form, at least for a relatively general simplified case. Although success has not been achieved, it has not yet been shown that this equation does not allow an analytical solution.

When the scatterers are much larger than the wavelength, the light is scattered predominantly within a small range of angles in the forward direction, and the transport equation can be simplified. A number of approaches to solve the transport equation in this case have been proposed [1,18]. We consider here the so called small angle approximation [1].

A unit vector specifying direction **s** can be expressed as

$$\mathbf{s} = \alpha\mathbf{x} + \beta\mathbf{y} + \gamma\mathbf{z}, \tag{2.62}$$

where **x**, **y**, and **z** are unit vectors in the respective directions, α, β, and γ are related to the spherical coordinates by

$$\alpha = \sin\theta\cos\varphi, \quad \beta = \sin\vartheta c\sin\varphi, \quad \gamma = \cos\theta. \tag{2.63}$$

Consider a plane wave incident on the slab in the direction **z**. In our approximation, angle θ is always small and, therefore, $\gamma \approx 1$. Thus, (2.61) can be written as

$$\frac{\partial}{\partial z} I(\rho,\mathbf{s}) + \mathbf{s}\cdot\nabla_t I(\rho,\mathbf{s}) = -\mu_t I(\rho,\mathbf{s}) + \mu_t \int_{-\infty}^{\infty}\int_{-\infty}^{\infty} I(\rho,\mathbf{s}')p(\mathbf{s}'-\mathbf{s})ds', \tag{2.64}$$

where

$$\mathbf{s} = \alpha\mathbf{x} + \beta\mathbf{y}, \quad \nabla_t = \frac{\partial}{\partial x}\mathbf{x} + \frac{\partial}{\partial y}\mathbf{y}, \quad \rho = \mathbf{r} - z\mathbf{z}, \tag{2.65}$$

and the integration over 4π in (2.61) is formally substituted by integration in the (**x**,**y**) plane. Although by the definition $\alpha^2+\beta^2 \le 1$, we can extend the integral over the entire (**x**,**y**) plane; because the major contribution to the integral comes from the region where α and β are small, the contribution from the range $\alpha^2+\beta^2>1$ is negligibly small, and we can extend the integration without introducing any significant error.

The solution of (2.64) can be found by using the Fourier transform method [17]. Multiplying equation (2.64) by $\exp(i\mathbf{k}\rho)$, and then integrating over all ρ, one can obtain:

$$\left(\frac{\partial}{\partial z} - i\mathbf{s}\mathbf{k} + \mu_t\right) I_1(z,\mathbf{k},\mathbf{s}) - \mu_t \int_{-\infty}^{\infty}\int I(z,\mathbf{k},\mathbf{s}')p(\mathbf{s}-\mathbf{s}')d\mathbf{s}' = 0, \tag{2.66}$$

with

$$I_1(z,\mathbf{k},\mathbf{s}) = \int_{-\infty}^{\infty}\int I(z,\rho,\mathbf{s})e^{i\mathbf{k}\rho}d\rho \tag{2.67}$$

is the Fourier transform of the specific intensity.

If we define

$$I_2(z,\mathbf{k},\mathbf{s}) = I_1(z,\mathbf{k},\mathbf{s})e^{(i\mathbf{k}\mathbf{s}-\mu)z}, \tag{2.68}$$

$$P(\mathbf{q}) = \int_{-\infty}^{\infty}\int p(\mathbf{s})e^{i\mathbf{s}\mathbf{q}}d\mathbf{s}, \tag{2.69}$$

$$F(z,\mathbf{k},\mathbf{q}) = \int_{-\infty}^{\infty}\int I_2(z,\mathbf{k},\mathbf{s})e^{i\mathbf{s}\mathbf{q}}d\mathbf{s}, \tag{2.70}$$

and take the Fourier transform of (2.66) with respect to **s**, we obtain the following first order differential equation for F:

$$\frac{d}{dz}F(z,\mathbf{k},\mathbf{q}) - \mu_t P(\mathbf{q}-\mathbf{k}z)F(z,\mathbf{k},\mathbf{q}) = 0. \tag{2.71}$$

The solution is

$$F(z,\mathbf{k},\mathbf{q}) = F(0,\mathbf{k},\mathbf{q})\exp\left(\int_0^z \mu_t P(\mathbf{q}-\mathbf{k}z')dz'\right). \tag{2.72}$$

Therefore, the solution of approximate transport equation (2.66) is obtained as inverse Fourier transform

$$I(z,\rho,\mathbf{s}) = \frac{1}{(2\pi)^4}\int\int d\mathbf{k}d\mathbf{q}F(z,\mathbf{k},\mathbf{q})e^{-i(\mathbf{k}\rho+\mathbf{s}\mathbf{q})+z(i\mathbf{s}\mathbf{k}-\mu_t)}. \tag{2.73}$$

This can be simplified to [1]

$$I(z,\rho,\mathbf{s}) = \frac{1}{(2\pi)^4}\int\int d\mathbf{k}d\mathbf{q}F_0(\mathbf{k},\mathbf{q}+\mathbf{k}z)K(z,\mathbf{k},\mathbf{q})e^{-i(\mathbf{k}\rho+\mathbf{s}\mathbf{q})} \tag{2.74}$$

where F_0 relates to the incident specific intensity I_i as

$$F_0(\mathbf{k},\mathbf{q}) = \int\int d\rho d\mathbf{s}I_0(\rho,\mathbf{s})e^{i(\mathbf{k}\rho+\mathbf{s}\mathbf{q})} \tag{2.75}$$

and

$$K(z,\mathbf{k},\mathbf{q}) = \exp\left\{-\int_0^z \mu_t\left(1-P(\mathbf{q}+\mathbf{k}(z-z'))\right)dz'\right\}. \tag{2.76}$$

Consider an incident beam with Guassian radial and angular distributions:

$$I_i(\mathbf{r},\mathbf{s}) = W\exp\left(-\alpha r^2\right)\exp\left(-\xi s^2\right), \tag{2.77}$$

with W a normalization coefficient. Since the solution (2.74) is valid only if the scattering is confined within a small solid angle, we do not introduce additional error if we approximate the phase function by

$$p(\mathbf{s}) = p_0\exp\left(-\beta s^2\right) \tag{2.78}$$

with a parameter β that defines the angular width of the forward peak. If chosen according to (2.21), β describes the forward peak quite accurately. However, as mentioned in section 2.1.2.1, in this case we disregard all the effects associated with light scattered in small angles but outside the forward peak. Since we are interested in integral properties of the phase function, it is important to choose the width of the Gaussian function, β, in such a way that it approximates the wing of the phase function as well. We should thus choose

$$\beta = \frac{c}{\left\langle \sin^2\theta \right\rangle} \tag{2.79}$$

with $c\approx 1$ and

$$\left\langle \sin^2\theta \right\rangle = 2\pi\int_{-1}^{1}\sin^3\theta p(\theta)d\theta \quad . \tag{2.80}$$

Substituting (2.77) into (2.75) we obtain

$$F_0(\mathbf{k},\mathbf{q}) = W\frac{\pi}{\xi\alpha}\exp\left(-\frac{q^2}{\xi}-\frac{k^2}{\alpha}\right) \tag{2.81}$$

and substituting (2.78) into (2.76) we find

$$P(\mathbf{q}) = p_0\frac{\pi}{\beta}\exp\left(-\frac{q^2}{\beta}\right). \tag{2.82}$$

Therefore,

$$K(z,\mathbf{k},\mathbf{q}) = \exp\left\{-\mu z + \frac{p_0\mu}{4\beta}\int_0^z\exp\left(-\frac{1}{\beta}\left(\mathbf{q}+\mathbf{k}(z-z')\right)^2\right)dz'\right\}. \tag{2.83}$$

The integral in (2.82) can not be evaluated analytically. However, it can be approximated by

$$\int_0^z \exp\left(-\frac{1}{\beta}\left(\mathbf{q}+\mathbf{k}(z-z')\right)^2\right)dz' = ze^{-\frac{q^2}{\beta}}. \tag{2.84}$$

Therefore, (2.74) becomes

$$I_f(z,\mathbf{r},\mathbf{s}) = \frac{W}{16\pi}\frac{1}{\alpha\xi}\exp\left(-\mu z\left(1-\frac{p_0}{4\beta}\right)\right)\int\int d\mathbf{q}d\mathbf{k}e^{-i(\mathbf{kr}-\mathbf{sq})}\exp\left(-\frac{q^2}{g(z)}-\frac{k^2}{\alpha}\right), \tag{2.85}$$

where we defined the function $g(z)$

$$g(z) = \left(\frac{1}{\xi}+\frac{p_0\mu}{4\beta^2}z\right)^{-1}. \tag{2.86}$$

Expression (2.85) can be simplified, and the transmitted specific intensity at point $\mathbf{r}$ in direction $\mathbf{s}$ is

$$I_f(z,\mathbf{r},\mathbf{s}) = \frac{W}{16\pi}\frac{1}{\alpha\xi}\exp\left(-\mu z\left(1-\frac{p_0}{4\beta}\right)\right)\exp\left(-g(z)s^2-\alpha r^2\right). \tag{2.87}$$

The signal detected in solid angle Ω_C by a detector with area S, I_f, is obtained by integrating (2.87):

$$I_f = \int_S d\mathbf{r}\int_{\Omega_c} ds I(L,\mathbf{r},\mathbf{s}). \tag{2.88}$$

If there is no dependence on phase angle ϕ,

$$I_f = \frac{\pi^2 W}{16\alpha\xi}\exp(-\mu L)\exp\left(-\mu\frac{\alpha L^2}{2\beta}\right)\left(1-\exp\left(-\frac{g(L)}{\xi_c}\right)\right) \tag{2.89}$$

where $\xi_C=\theta_C^{-1}$ is the inverse width of the collection angle.

For the practically important case when

$$\frac{L^2\alpha}{2\beta} << 1$$

(2.89) is reduced to

$$I_f = \frac{\pi^2 W}{16\alpha\xi}e^{-\tau}\left\{1-\exp\left[-\frac{\xi}{\xi_c}\left(1-\tau\frac{\xi}{\beta}\right)\right]\right\}. \tag{2.90}$$

This signal should contain the oscillatory component. However, its amplitude, in contrast to that obtained using first order approximation for $\tau \leq 1$, starts to decrease for $\tau \geq \frac{\beta}{\xi}$. This can be understood by noting that τ is the most probable number of collisions of a photon has the scatterers inside the slab. In every scattering event the photon changes its previous direction by $\frac{1}{\sqrt{\beta}}$. Thus, after $\tau_c = \frac{\beta}{\xi}$ collision the photons "forget" their initial angular distribution. When the number of scattering events is larger than τ_c, randomization takes place. If we increase τ even further, we achieve complete diffusion. Diffusely transmitted light lacks the oscillatory component. We should note, however, that the resultant signal contains some oscillatory component even for large τ, because there are always some particles near the surface that scatter light just before it emerges, and the scattering by these particles results in the formation of an oscillatory component.

2.2.3 Important results from this section

In this section the light reflectance from a slab of large particles, simulating epithelial layer covering surfaces of the most biological tissues, was considered. It was shown that the wavelength dependent oscillations of the cross section give rise to corresponding oscillatory components in the reflectance from the tissue.

There are two effects contributing to the oscillatory component in reflectance – (1) backscattering of the incident light from the particles inside the slab and (2) scattering of the "diffusive" light returning toward the surface when it propagates through the slab. In section 2.2.1 the contribution of backscatteringn was considered. The fraction of the reflectnace associated with backscattering was obtained (2.39) in the case when the optical distance $\tau \leq 1$ which is valid for many practical applications. Expression (2.40) showed that the backscattered signal has an oscillatory component proportional to $-\tau$.

In section 2.2.2 the contribution of the scattering of the "diffusive" light was discussed. Two cases were considered: (1) $\tau \leq 1$ -- section 2.2.2.1, and (2) large τ -- section 2.2.2.2 (less

practically important case). The intensity transmitted through the slab was obtained (2.55). Expression (2.56a) presented the transmitted signal in a practically important case of small collection and illumination angles. This expression will be used in the following section. Limit of small τ was considered as well (2.59). It was shown that the transmitted signal has an oscillatory component proportional to $-\tau$, just like in case of backscattering.

Thus both effects are additive, and reflectance from a biological tissue covered by epithelium exhibits wavelength dependent oscillations proportional to $-\tau$. Since the optical distance τ is determined by the size distribution of the scatterers inside the slab, $N(l)$ (2.37), the size distribution can be obtained by analyzing the oscillatory component. To achieve this, an inversion technique is necessary.

2.3 Inversion of the oscillatory component to determine size distribution of the scatterers

The reflectance $R(\lambda)$ from a tissue covered by a thin slab of epithelial tissue containing nuclei with size distribution $N(l)$ [number of nuclei per unit area (mm^2) and per unit interval of nuclear diameter (μm)] collected by an optical probe with acceptance angle Ω_C consists of backward scattered photons and photons passing through the epithelium from the underlying tissues. The contribution of backscattered photons is given by (2.56a). For small solid angles Ω_i and Ω_C the expression in the integral in (2.56a) can be expanded in $1-\cos\theta<<1$ (see a similar expansion in section 2.2.2.1) and the component of the reflectance associated with backscattering is approximated by

$$R_b(\lambda) = \frac{\langle I_b \rangle_{\Omega_c}}{\langle I_i \rangle_{\Omega_i}} = \frac{1 - e^{-\tau(\lambda)}}{\langle I_i \rangle_{\Omega_i}} \left\langle \left\langle I_i(\lambda, -\mathbf{s}') p(\lambda, \mathbf{s}, \mathbf{s}') \right\rangle_{\Omega_i} \right\rangle_{\Omega_c}, \tag{2.91}$$

where I_i is the specific intensity of the incident light delivered in solid angle Ω_I, and $\langle f(\mathbf{s},\mathbf{s}') \rangle_{\Omega} = \int_{\Omega} f(\mathbf{s},\mathbf{s}') d\mathbf{s}'$ for any function f and solid angle Ω.

The component of reflectance formed by photons transmitted through epithelium from underlying layers can be obtained in the same approximation from (2.56a):

$$R_f(\lambda) = \frac{\langle I_f \rangle_{\Omega_c}}{\langle I_i \rangle_{\Omega_i}} = \frac{\langle I_d \rangle_{2\pi}}{\langle I_i \rangle_{\Omega_i}} e^{-\tau(\lambda)} + \frac{1 - e^{-\tau(\lambda)}}{\langle I_i \rangle_{\Omega_i}} \left\langle \langle I_d(\lambda, \mathbf{s}') p(\lambda, \mathbf{s}, \mathbf{s}') \rangle_{2\pi} \right\rangle_{\Omega_c}, \qquad (2.92)$$

where I_d is the specific intensity of light emerging from the underlying tissue.

Thus, the total reflectance $R=R_b+R_f$ is given by

$$\frac{R(\lambda)}{\overline{R}(\lambda)} = e^{-\tau(\lambda)} + \frac{1 - e^{-\tau(\lambda)}}{\langle I_d(\lambda, \mathbf{s}) \rangle_{\Omega_c}} \left\langle \langle I_i(\lambda, -\mathbf{s}') p(\lambda, \mathbf{s}, \mathbf{s}') \rangle_{\Omega_i} + \langle I_d(\lambda, \mathbf{s}') p(\lambda, \mathbf{s}, \mathbf{s}') \rangle_{2\pi} \right\rangle_{\Omega_c}, \qquad (2.93)$$

where the quantity $\overline{R}(\lambda)$ is the reflectance of the diffusive background

$$\overline{R}(\lambda) = \frac{\langle I_d(\lambda, \mathbf{s}) \rangle_{\Omega_c}}{\langle I_i(\lambda, \mathbf{s}) \rangle_{\Omega_i}}. \qquad (2.94)$$

The optical distance $\tau(\lambda)$ depends on the nuclear size distribution as

$$\tau(\lambda) = \int \sigma_s(\lambda, l) N(l) dl,$$

and the scattering phase function is given by

$$p(\lambda, \mathbf{s}, \mathbf{s}') = \frac{1}{\tau(\lambda)} \int p(\lambda, l, \mathbf{s}, \mathbf{s}') \sigma_s(\lambda, l) N(l) dl.$$

The first term in (2.91) describes the attenuation of the diffuse background, and the terms in brackets describe backscattering of the incident light and forward scattering of diffusive background by the epithelial cell nuclei, respectively.

As we saw in the previous section, the forward scattering term oscillates in phase with $\tau(\lambda)$, as required by the optical theorem, whereas the backscattering term is out of phase. Thus, the epithelial nuclei introduce a oscillatory component in the reflectance with a wavelength dependence similar to that of the cross section. Its periodicity is approximately proportional to nuclear diameter, and its amplitude is a function of the size and number of nuclei in the epithelium. These quantities can be determined by analyzing the reflectance $R(\lambda)$.

Neglecting the square term in (2.12), the cross section $\sigma_S(\lambda, l)$ of a large particle can be written as

$$\sigma_s(\lambda,l) = \frac{\pi l^2}{2}\left(1-\gamma(\lambda,l)\right) \tag{2.95}$$

where $\gamma(\lambda,l)$ is a oscillatory component of the cross section,

$$\gamma(\lambda,l) = 2\frac{\sin\left(k(\lambda)l\right)}{k(\lambda)l} \tag{2.96}$$

and k is the effective wavenumber

$$k(\lambda) = \frac{2\pi\left(n_2 - n_1\right)}{\lambda}, \tag{2.96}$$

with n_2 and n_1 the refractive indexes of the scatterer, nucleus, and the surrounding medium, cytoplasm. Since

$$\left\langle\left\langle I_d(\lambda,\mathbf{s}')p(\lambda,l,\mathbf{s},\mathbf{s}')\right\rangle_{2\pi}\right\rangle_{\Omega_c} = f_0 + f_1\left(1-\gamma(\lambda,l)\right) \tag{2.97}$$

where the positive parameters f_0 and f_1 depend on the angle Ω_c and can be determined numerically, the forward scattering term in (2.91) can be written as

$$\left\langle\left\langle I_d(\lambda,\mathbf{s}')p(\lambda,\mathbf{s},\mathbf{s}')\right\rangle_{2\pi}\right\rangle_{\Omega_c} = \frac{\pi}{2\tau(\lambda)}\int dlN(l)l^2\left(1-\gamma(\lambda,l)\right)\left(f_0 + f_1\left(1-\gamma(\lambda,l)\right)\right). \tag{2.98}$$

For the backscattering term,

$$\left\langle\left\langle I_t(\lambda,\mathbf{s}')p(\lambda,l,\mathbf{s},\mathbf{s}')\right\rangle_{\Omega_t}\right\rangle_{\Omega_c} = b_0 - b_1\left(1-\gamma(\lambda,l)\right) \tag{2.99}$$

and, therefore,

$$\left\langle\left\langle I_t(\lambda,\mathbf{s}')p(\lambda,\mathbf{s},\mathbf{s}')\right\rangle_{\Omega_t}\right\rangle_{\Omega_c} = \frac{\pi}{2\tau(\lambda)}\int dlN(l)l^2\left(1-\gamma(\lambda,l)\right)\left(b_0 - b_1\left(1-\gamma(\lambda,l)\right)\right). \tag{2.100}$$

For all large l, $|\gamma(\lambda,l)|<<1$ and

$$\frac{\pi}{2\tau}\int dlN(l)l^2\gamma(\lambda,l) = \frac{\Gamma(\lambda)}{\tau_0} \tag{2.101}$$

where we have defined

$$\Gamma(\lambda) = \frac{\pi}{2}\int dlN(l)l^2\gamma(\lambda,l), \quad \tau_0 = \frac{\pi}{2}\int dlN(l)l^2. \tag{2.102}$$

The function $\Gamma(\lambda)$ represents the oscillatory component introduced by the epithelium, and τ_0 is twice the total geometrical cross section of the epithelial nuclei per unit area. Substituting (2.98) and (2.100) into (2.93), we obtain for $\tau_0<<1$:

$$\frac{R(\lambda)}{\bar{R}(\lambda)} - 1 \approx q\Gamma(\lambda) \tag{2.103}$$

with parameter $q = 1 - f_0 - f_1 - b_0 + b_1$. Thus, if we can measure the reflectance $R(\lambda)$ and the diffusive background $\bar{R}(\lambda)$, we can find $\Gamma(\lambda)$.

Function $\Gamma(\lambda)$ is the integral transform with kernel $\gamma(\lambda,l)$ of an unknown function $N(l)$. We need to find such inverse transform V that

$$V[\Gamma(\lambda),l] = N(l). \tag{2.104}$$

In this case, the nuclear size distribution $N(l)$ can be found as the transform of the function $\frac{R(\lambda)}{\bar{R}(\lambda)}$, which is to be determined from the measurements:

$$N(l) = \frac{1}{q} V\left[\frac{R(\lambda)}{\bar{R}(\lambda)} - 1, l\right]. \tag{2.105}$$

Given that $\gamma(\lambda,l) = 2\frac{\sin(k(\lambda)l)}{k(\lambda)l}$ and

$$\int_0^\infty \sin kl \sin kl' dk = \frac{\pi}{2}\delta(l-l'), \tag{2.106}$$

the integral transform V is related to the Fourier transform

$$V[\Gamma,l] = \frac{2}{\pi^2 l}\int_0^\infty \Gamma(k)\sin(kl)kdk = \frac{8(n_2-n_1)^2}{l}\int_0^\infty \frac{\Gamma(\lambda)}{\lambda^3}\sin\left(\frac{2\pi(n_2-n_1)l}{\lambda}\right)d\lambda. \tag{2.107}$$

In practice, however, the reflectance $R(\lambda)$ and, therefore, $\Gamma(\lambda)$, are measured only in some wavelength range from λ_{min} to λ_{min}. $\Gamma(\lambda)$ vanishes for wavelengths smaller than

$$\lambda_1 \cong 0.1\pi l_{min}(n_2 - n_1), \tag{2.108}$$

where l_{min} is the diameter of a smallest nucleus present in the epithelium. For l_{max}=5μm, λ_1≈120nm. $\Gamma(\lambda)$ does not have oscillatory behavior for wavelengths large than

$$\lambda_2 \cong \pi l_{max}(n_2 - n_1), \tag{2.109}$$

where l_{max} is the diameter of the largest nucleus. For l_{max}=15 μm, λ_2≈2800nm. Thus, if we measure $R(\lambda)$ for all $\lambda \subset [\lambda_1,\lambda_2]$, we can apply transform (2.107), integrating from λ_1 to λ_2 rather than from zero to infinity. However, if the reflectance $R(\lambda)$ is measured for optical

wavelengths only (from λ_{min}=360nm to λ_{max}=700nm for example in the experiments discussed in Chapter 3), than

$$V'[\Gamma, l] = \frac{2}{\pi^2 l} \int_{k_{min}}^{k_{max}} \Gamma(k) \sin(kl) k dk . \tag{2.110}$$

with $k_{min} = \frac{2\pi(n_2 - n_1)}{\lambda_{max}}$ and $k_{max} = \frac{2\pi(n_2 - n_1)}{\lambda_{min}}$.

Consider the following important example. If all the nuclei have the same diameter l_0, $N(l)=N_0\delta(l-l_0)$ and

$$V'[\Gamma, l] = \frac{N_0}{\pi} \frac{\sin(k_{max}(l - l_0)) - \sin(k_{min}(l - l_0))}{l - l_0} - \frac{N_0}{\pi} \frac{\sin(k_{max}(l + l_0)) - \sin(k_{min}(l + l_0))}{l + l_0} . \tag{2.111}$$

The function $V(l)$ has a number of peaks, with the main peak at $l=l_0$. The broader the range $[k_{min}, k_{max}]$, the more prominent and narrower the main peak. $V'(l)$ is shown in Fig. 2.13 for l_0=10μm and λ_{min}=360nm, λ_{max}=700nm. The false peaks may be mistaken for peaks from actual nuclei. Therefore, to invert $\Gamma(\lambda)$ we need to modify (2.107). There are a number of ways to achieve this. One may extend $\Gamma(\lambda)$ in a broader wavelength range using some numerical algorithms and then apply (2.107). We, however, consider another way to perform the inverse transform.

Let us modify the integral transform (2.110):

$$V_m[\Gamma, l] = \frac{2}{\pi^2 l} \left| \int_0^{\Delta k} \Gamma(k) \exp(ikl)(k + k_{min}) dk \right| \tag{2.112}$$

with $\Delta k = 2\pi(n_2 - n_1)\left(\frac{1}{\lambda_{min}} - \frac{1}{\lambda_{max}}\right)$. The modified transform has the exponential kernel, instead of the sine kernel used in the transform (2.110) and the range of integration is shifted for convenience. Substituting in, $N(l)=N_0\delta(l-l_0)$, we obtain

$$V_m[\Gamma, l] \approx \frac{N_0}{\pi} \frac{\sin \Delta k(l - l_0)}{l - l_0} . \tag{2.113}$$

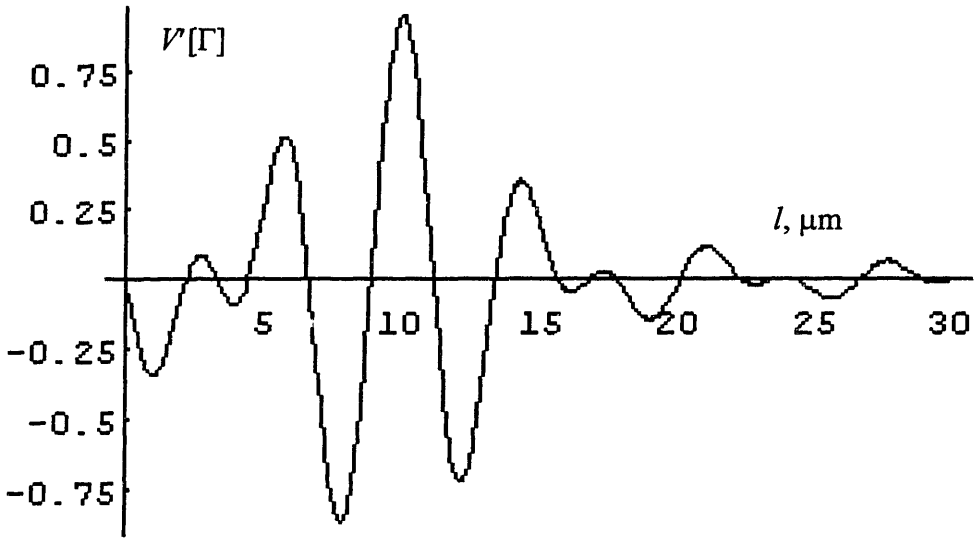

Figure 2.13. Inverse operator $V[\Gamma(\lambda),l]$. The function $\Gamma(\lambda)$ was calculated for the nuclear size distribution $N(l)=\delta(l-l_0)$, $l_0=10\mu m$.

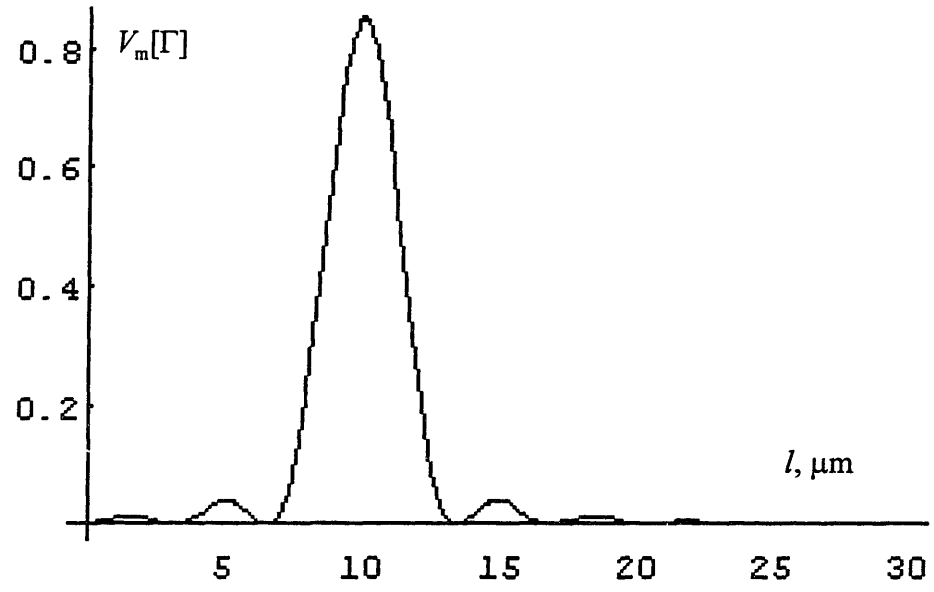

Figure 2.14. Inverse operator $V_m[\Gamma(\lambda),l]$. The function $\Gamma(\lambda)$ was calculated for the nuclear size distribution $N(l)=\delta(l-l_0)$, $l_0=10\mu m$.

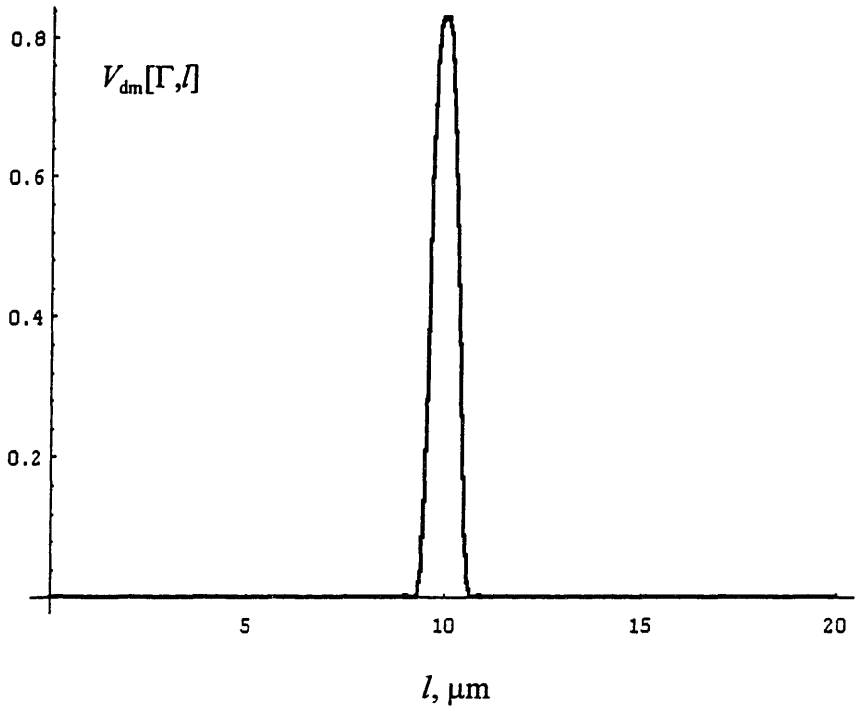

Figure 2.15. Inverted nuclear size distribution $V_m[l]$ after deconvolution with the Gaussian function.

Thye function $V_m[\Gamma,l]$ is shown in Fig. 2.14. The peak at $l=l_0$ is more prominent than that of $V'[\Gamma,l]$. Noticing that the main peak of $V_m[\Gamma,l]$ can be approximated as a Gaussian function with standard deviation σ=1.1μm:

$$A\exp\left(-\frac{x^2}{2\sigma^2}\right),$$

with an appropriate normalization parameter A, we can further increase the resolution of the inverse transform, deconvolving $V_m[\Gamma,l]$ with the Gaussian curve:

$$V_{dm}[\Gamma,l]=\frac{\alpha}{\pi}\int e^{\alpha(l-il')^2}V_m[\Gamma,l']dl', \qquad (2.114)$$

with α=0.4μm^{-2} (which corresponds to the σ=1.1μm of the deconvolving Gaussian curve). The resulting size distribution, $V_{dm}[l]$, is shown in Fig. 2.15. Its width is less than 0.3μm. Such accuracy of determination of the nuclear size distributions is sufficient (see experimental results presented in Chapter 3).

Thus, the nuclear size distribution can be determined as a transform of the reflectance $R(\lambda)$:

$$V_m[\Gamma,l]=\frac{2}{\pi^2 ql}\left|\int_0^{\Delta k}\left(\frac{R(k)}{\bar{R}(k)}-1\right)\exp(ikl)(k+k_{\min})dk\right|. \tag{2.115}$$

If τ_0 is not small relative to unity, but rather in the same order of magnitude, and $\tau_0|\gamma(\lambda,l)|<<1$, (2.103) is no longer valid. Substituting (2.98), (2.100), and (2.101) into (2.93), and introducing a new operator acting on an arbitrary function f

$$U[f(x)]=\frac{\pi}{2}\int f(x)x^2dx, \tag{2.116}$$

we obtain the following equation

$$U\left[V\left[\frac{R(\lambda)}{\bar{R}(\lambda)}-1\right]\right]=\tau_0 e^{-\tau_0}\left(1-f_0-b_0\right)+\left(1-e^{-\tau_0}\right)\left(b_1-f_1\right). \tag{2.117}$$

This transcendental equation should be solved for τ_0.

Applying operator V to (2.91) we obtain

$$V\left[\frac{R(\lambda)}{\bar{R}(\lambda)}-1\right]=N(l)\left\{e^{-\tau_0}\left(1-f_0-b_0-\left(b_1-f_1\right)\tau_0^{-1}\right)+\left(b_1-f_1\right)\tau_0^{-1}\right\}. \tag{2.118}$$

To determine the nuclear size distribution in this case, we need first to find τ_0 from equation (2.117), substitute it into (2.118), and find $N(l)$.

References

1. A. Ishimaru, Wave Propagation and Scattering in Random Media (Academic Press, Orlando, 1978).
2. V. Twerski, J. Opt. Soc. Am., **60**, 1084 (1970).
3. Y. N. Barabanenkov, Y.A. Kravtsov, S.M. Rytov, V.I. Tatarski, Sov. Phys. Usp., **13**, 551 (1971).
4. F.J. Dyson, J. Opt. Soc. Am., **65**, 551 (1975).
5. N. Metropolis, S. Ulam, J. Am. Statist. Asso., **44**, 335 (1949).
6. J. Beuthan, O. Minet, J. Helfmann, M. Herrig, and G. Muller, Phys. Med. Biol. **41**, 369 (1996).
7. P. M. A. Slot, A.G. Hoekstra, and C.G. Figdor, Cytometry **9**, 636 (1988).
8. R.S.Cotran, S.L. Robbins, V. Kumar, *Robbins Pathological Basis of Disease* (W.B. Saunders Company, Philadelphia, 1994).
9. R.G. Newton, *Scattering Theory of Waves and Particles* (McGraw-Hill Book Company, New York, 1969).
10. L.D. Landau, *Quantum Mechanics* (Academic Press, New York, 1980)
11. H.C. van de Hulst, *Light Scattering by Small Particles* (Dover Publications, New York, 1957).
12. J.D. Jackson, *Classical Electrodynamics*, (John Wiley & Sons, New York, 1975).
13. G. Mie, Annalen der Physik, Band 25, No3 (1908).
14. D. W. Fawcett, A Textbook of Histology, (Charman & Hall, New York, 1994).
15. M.A. O'Leary, D.A. Boas, B. Chance, and A.G. Yodh, Phys. Rev. Lett., **69**, 2658-2661, (1992).

16. I.D. Campbell, R.A. Dwek, *Biological Spectroscopy*, (Baenjamin & Cummings Publishing, Mento Park, 1984).

17. P.M. Morse and H. Feshbach, *Methods of Theoretical Physics* (McGraw-Hill, New York, 1953).

18. S. Chandrasekhar, *Radiative Transfer*, (Oxford Univ. Press, London, 1960).

19. M. Kerker, *The Scattering of Light*, (Academic Press, New York, 1969).

20. M. Abramovitz and I. Stegun, Handbook of Mathematical Functions, (Dover Publications, New York, 1972).

Chapter 3

Observation of oscillatory fine structure in the reflectance from biological tissue

3.1 Oscillatory component in reflectance from a biological tissue

3.1.1 Oscillatory fine structure as a signature of epithelial cell nuclei

In the previous chapter we showed that the reflectance spectrum from a biological tissue covered by epithelium should exhibit a fine oscillatory component resulting from light scattering by the cell nuclei present in this layer. This effect should not be limited to epithelial cells. The oscillatory component may be seen in the reflectance from virtually any type of biological tissue having a rich cellular content. The only stipulation is the absence of complete diffusion inside the tissue. The oscillatory structure should be observed not only in reflectance from biological tissues, but also in reflectance from any layer that contains scatterers large comparing to the wavelength (a solution of large polystyrene beads, for example). Since most of the organs in the human body are covered by epithelium, we can say that the oscillatory component in reflectance has an epithelial origin.

By analyzing the oscillatory component, one can determine the size distribution of the scatterers that produce it, in the case of a biological tissue – the cell nuclei. The ability to measure nuclear size distributions *in vivo* (*in vivo* means inside the body, without tissue

removal) has potentially valuable applications in medicine, since enlarged nuclei are primary indicators of cancer and the precancerous condition, dysplasia [1].

Methods to diagnose cancer at an early stage are essential for cancer prevention and therapy. Many types of cancer grow from the epithelial tissues which cover the inner and outer surfaces of the body. Many of those, for example cancer in the gastrointestinal tract, progress through the stage of dysplasia. Dysplasia can be defined as neoplastic tissue which, although not yet malignant, has the potential to become malignant, i.e. dysplasia is a precursor of malignancy. If diagnosed at this stage, most tumors are curable (90%-100% depending on the organ) [1]. In the case of gastrointestinal tumors, the diagnosis is based on endoscopy. However, dysplastic tissue is not always endoscopically apparent. In this case, detection of dysplasia in the gastrointestinal tract relies on random sampling for this "invisible" malignant precursor. Hc ver, samples selected via random biopsy a have high probability to miss the dysplastic changes. In addition, in some cases biopsy samples cannot be taken. Instead of random biopsy, some optical techniques, such as reflectance spectroscopy, might be useful. Most human organs can be diagnosed by means of optical techniques. The gastrointestinal tract is a particularly good example, since it is easily accessible by optical probes which can be inserted into one of the channels of a conventional endoscope. In this chapter we study to the case of gastrointestinal epithelial dysplasia, and particularly dysplasia in Barrett's esophagus.

Adenocarcinoma of the esophagus arises almost exclusively in the settings of metaplastic columnar epithelial cells in the esophagus, termed "Barrett's esophagus", which is a complication of long-standing gastric acidal reflux. In this condition, the distal squamous epithelium is replaced by columnar epithelium consisting of one cell layer which resembles that of the large intestine. There is a strong evidence of progression from Barrett's esophagus to associated dysplasia to invasive carcinoma. Patients with Barrett's esophagus have approximately forty times greater chance to develop esophageal adenocarcinoma than the general population. The 5 years survival of patients with esophageal adenocarcinoma is less than 15% and, unfortunately, endoscopic surveillance of patients with Barrett's esophagus has not resulted in reduction of esophageal cancer mortality. The most likely explanation for this is that surveillance of Barrett's esophagus is based on random biopsy, because dysplasia

occurring in the esophagus cannot be seen with standard endoscopic imaging. This procedure can sample only about 0.3% of the tissue at risk. Thus, there is tremendous potential for sampling error.

The application of reflectance spectroscopy to diagnose dysplasia in Barrett's esophagus is limited by the fact that the primary alterations in the tissue occur in the epithelium which can be one cell thick (~20-30μm), while the reflectance spectrum is mostly formed in the deeper tissue layers. One of the most prominent features of a dysplastic epithelium is the presence of enlarged, hyperchromatic, and crowded nuclei [1]. (Nuclear hyperchromatism means that the nuclei appear darker when stained on a glass slide.) These changes in nuclei size and spatial distribution are the primary markers used by pathologists to diagnose dysplasia. No significant changes in other tissue layers are observed.

Three most important diagnostic features of dysplastic epithelium -- enlarged, hyperchromatic, and crowded nuclei -- can be measured spectroscopically. Determination of the nuclear size distribution using the technique based on the analysis of the oscillatory component of the reflectance can provide a direct evidence for the presence of the enlarged nuclei. Nuclear hyperchromatism indicates an increase of nuclear DNA concentration and, consequently, increase of nuclear refractive index (the nucleus is a solution of DNA, proteins, and small molecules in water; the higher the concentration of the non-water components, the higher the refractive index). As shown in Chapter 3, changes in refractive index can be determined by the analysis of the oscillatory component. Finally, the fact that the nuclei appear crowded means that their concentration, $\int N(l)dl$, is increased. This can be determined from the nuclear size distribution as well. Thus, the measurement of the oscillatory component in reflectance spectra can give crucial information to diagnose dysplastic changes in epithelial tissues.

In conclusion, we should mention that there are many examples other than diagnosis of cancer and precancerous conditions where the measurement of size distributions of the scatterers present in some thin surface layer might be important. These include diagnosis of inflammation, regeneration, and differentiation in biological tissues, diagnosis of some nervous disorders, studies with cell cultures, as well as applications not related to biology.

3.1.2 Formation of the oscillatory component in reflectance from a tissue of a hollow organ. Esophagus as an example

3.1.2.1 Histological organization of the tissue of a hollow organ

To understand how light interacts with the tissue of a hollow organ [organs of the gastrointestinal tract (intestine, esophagus, stomach), respiratory tract (bronchi), genitourinary tract (bladder, cervix), etc.], it is helpful to consider some general features of its histological organization. We consider the gastrointestinal (GI) tract as an example, other hollow organs generally exhibits the same features.

The wall of the GI tract is covered by a layer of cells called the epithelium. This tissue layer is 20 μm to 300μm thick, depending on the part of the tract. The intestines, stomach, and Barrett's esophagus are covered by an epithelium layer one cell thick; normal esophagus and mouth have squamous stratified epithelium that can be as thick as 300μm. The epithelium is supported by relatively acellular and highly vascular loose connective tissue, lamina propria, which can be up to 500μm in thickness and contains a network of collagen and elastic fibers, and a variety of white blood cells [2]. Beneath it there is a muscular layer, the muscularis mucosae, which usually consists of two (intestines, middle esophagus) or three (stomach) tenuous layers of smooth muscle cells. The proximal esophagus is an exception -- muscularis mucosae is represented only by scattered fascicles of smooth muscle cells. In the distal esophagus near the stomach, the muscularis mucosae can attain a thickness of 200-400 μm. Epithelium, lamina propria, and muscularis mucosae organize mucosal tissue. Beneath the mucosa lies another layer of moderately dense connective tissue called the submucosa (400-600μm thick), which contains many small blood vessels and abundant collagen and elastic fibers. The overall thickness of mucosal and submucosal layers is about 1mm. Since a characteristic penetration depth of optical radiation in biological tissue does not usually exceed 1mm, it is sufficient to limit our consideration to those layers. Figure 3.1 shows the mucosa of Barrett's esophagus with and without dysplasia.

Figure 3.1 Mucosa of Barrett's esophagus, showing dusplastic as well as non dysplastic epithelium. Cell nuclei are colored deep blue by the H&E stain. Epithelial cells and the layer of lamina propria with scattered white and red blood cells are seen. [12]

When we discussed the oscillatory component in section 2, two simplifications were made: the surface of the tissue was assumed to be flat, and the scatterers were assumed to have spherical shape. In Barrett's esophagus, (1) the mucosa is folded into so-called crypts (Fig.3.1) and (2) the nuclei are prolonged spheroids rather than perfect spheres. However, these features of realistic tissues do not alter the above conclusions.

(1) Since photons scattered from the uppermost cell nuclei only contribute to the oscillatory component in reflectance signal, the non-flat architecture of the crypts and irregularities of the surface do not offend the scattering process and do not alter the oscillatory component.

(2) Most cell nuclei are oriented in such a way that their long axis is perpendicular to the basal surface of the cell. Because of the folding of the epithelium, the nuclear orientation relative to the direction of the propagation of the incident light varies depending on the position of a cell in a crypt. Thus, all the conclusions made in section 2 still hold (l is an average diameter of a nucleus in this case).

3.1.2.2 Formation of the oscillatory fine structure

Consider the formation of a reflectance signal in a mucosal tissue such as esophagus. When the collimated incident light propagates through the epithelium, some part of it is scattered backward and collected, while the rest penetrates deeply into the tissue where it undergoes multiple diffuse scattering and absorption. Several studies have shown that collagen is a strong scatterer, and that hemoglobin, present in the blood vessels perfusing the tissue, is the predominant absorber of visible light [3]. Small particle scattering and hemoglobin absorption result in the formation of the general shape of the spectral curve. Its analysis makes it possible to obtain important tissue characteristic such as hemoglobin concentration, oxygenation, and the characteristic size of scatterers present in the tissue [4]. However, since in dysplasia the only significant change occurs in the epithelium, the knowledge of the parameters associated with other tissue layers does not give us much information for diagnosis of dysplasia.

Returning to the tissue surface, diffusely reflected light passes again through the epithelium where it is again scattered by nuclei. However at that time, forward scattered

photons are collected. These processes result in the formation of the oscillatory component in the reflectance signal. Its period is inversely proportional to $l(n-1)$, where l is the diameter of the nucleus and n is the refractive index of the nucleus relative to that of surrounding cytoplasm. Thus, the periodicity increases with nuclear size and is higher for enlarged dysplastic nuclei than for non-dysplastic nuclei. In addition, its amplitude is proportional to the number of scatterers present. By measuring the periodicity and amplitude, we can determine the diameter and the number of the nuclei. Thus, the reflectance signal consists of a "coarse" structure, which is a result of diffusive scattering and absorption, and a fine oscillatory structure which is a "fingerprint" of the cell nuclei. However, in order to extract the fine structure the coarse structure (diffuse background) must be eliminated first. To make this possible, a physical model incorporating the effects of the diffuse scattering and hemoglobin absorption has been developed (see below).

A number of cell types are present in the mucosa [2]. These include epithelial cells, cells of connective tissue, inflammatory white blood cells, and erythrocytes. Epithelium is always the uppermost layer of the tissue, while most non-epithelial cells are distributed beneath it. Although the scattering cross sections of many cell nuclei should exhibit an oscillatory functional dependence on wavelength, not every nucleus can participate in the formation of the fine structure. The light scattered from a nucleus inside a diffusive region of tissue, inside the lamina propria for example, cannot result in the modulation of the resulting reflectance signal, because photons come to it from all possible directions, they are randomized after that scattering, and information about the scattering event is missed. Thus, non-epithelial layers of tissue produce the coarse structure of the reflectance signal, and only the epithelial layer is responsible for the fine structure.

3.1.2.3 Subtraction of the diffuse background

To determine the nuclear size distribution $N(l)$ using (3.115) one needs to know the reflectance signal $R(\lambda)$, which is measured experimentally, and the so-called diffuse background $\overline{R}(\lambda)$ (2.94). The fine structure component can be less than 5% of the total signal and is ordinarily masked by this background of diffusely scattered light from underlying tissue, which itself exhibits spectral features due to absorption and scattering [Fig. 3.7(a)]. In order to observe the fine structure, this background must be removed using an appropriate model. The diffusive reflectance from biological tissues will be discussed in details in [11], and only discuss it briefly here.

The spectral features of the diffuse background are dominated by the characteristic absorption bands of hemoglobin [3]. The absorption length, μ_a^{-1} [13], ranges from 0.5 to 250 mm, and the typical effective scattering length, $(\mu_s')^{-1}$, is 0.1 to 1 mm [3]. Thus, scattering and absorption are of the same order, and both have to be taken into account in modeling the background. The functional dependencies of the absorption coefficients μ_a [13] and the scattering coefficient μ_s' [3] on wavelength are shown in Fig. 3.2.

We employed a simple physical model to describe this background [14]. Light incident on the tissue is assumed to be exponentially attenuated. At any given depth, z, an amount of light proportional to the reduced scattering coefficient μ_s' is scattered back towards the surface and further exponentially attenuated. Since light attenuation depends on both scattering and absorption, the attenuation coefficient is assumed to be the sum of absorption coefficient μ_a and effective scattering coefficient $\mu_s^{(e)} = \beta\mu_s'$. The parameter β was determined by comparison with more accurate models of light transport and Monte Carlo simulations, and was found to be $\beta \cong 0.07$ [6,7]. Since light only penetrates ~1 mm into the tissue, most of the diffusely scattered return light originates in the connective tissue layers. We thus modeled the tissue as a two layer medium with thin epithelium on top of a thick diffusive layer.

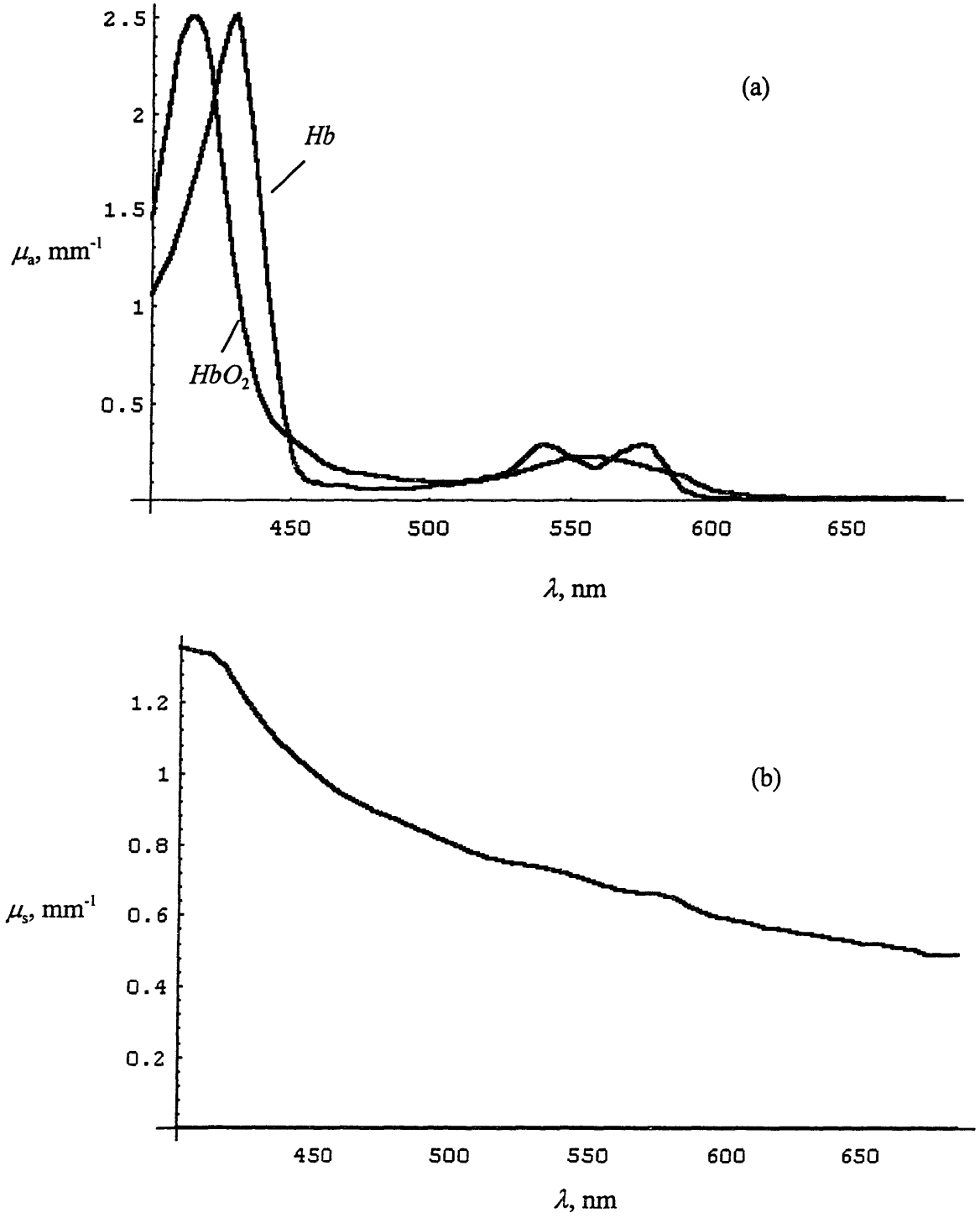

Figure 3.2 (a) Absorption coefficient $\mu_a(\lambda)$ of a oxygenated (HbO_2) and deoxygenated (Hb) forms of hemoglobin [13]. (b) Reduced scattering coefficient $\mu_s(\lambda)$ measured in colon tissue [3].

We then obtain the following approximate expression for the diffusive light from underlying tissue impinging on the epithelial cell layer [5]:

$$I_d(\lambda,\mathbf{s}) = F(\mathbf{s})\langle I_i(\lambda,\mathbf{s})\rangle_{\Omega_i} \frac{1-\exp[-(\mu_s^{(e)}+c\mu_a)L]}{1+c(\mu_a/\mu_s^{(e)})} \tag{3.1}$$

and the corresponding background reflectance

$$\overline{R}(\lambda) = \frac{1-\exp[-(\mu_s^{(e)}+c\mu_a)L]}{1+c(\mu_a/\mu_s^{(e)})} R_0, \tag{3.2}$$

where the function

$$F(\mathbf{s}) = \frac{\Delta+\cos\theta}{\pi(2\Delta+1)} \tag{3.3}$$

describes the angular dependence of light emerging from the mucosal layer, **s** is a unit vector pointing outward from the tissue surface in an arbitrary direction, θ is the angle between vector **s** and normal to the surface of the tissue pointing outward, Δ=0.7104 [8], parameter L is proportional to the effective thickness of the diffusive layer, parameter c is proportional to the concentration of hemoglobin (which is the predominant absorber) to the concentration of the scatterers in the diffusive layer, and R_0 is the normalization parameter that depends on the probe size, angular aperture, distance from the probe to the tissue surface, etc. Because both oxygenated and de-oxygenated hemoglobin are present, the total hemoglobin absorption is modeled as

$$\mu_a = (1-\alpha)\mu_a^{(Hb)} + \alpha\mu_a^{(HbO_2)} \tag{3.4}$$

with oxygen saturation parameter α ($0 \le \alpha \le 1$). Despite the fact that this model is approximate, it describes the reflectance from mucosal tissues of the GI tract quite accurately (Fig. 3.7(a)).

Thus, to find nuclear size distribution $N(l)$, one needs to complete three steps.

(1) Measure the reflectance from the tissue $R(\lambda)$.

(2) Determine the corresponding diffuse background $\overline{R}(\lambda)$ by fitting (3.2) to the broad features of $R(\lambda)$ by varying the parameters c, α, L, and R_0. Note that the absorption coefficient μ_a and scattering coefficient μ_s' are functions of wavelength and they are not varied during the fitting procedure. Our studies showed that this simple model (3.2) was

able to describe the measured reflectance spectra from human esophageal tissues quite accurately (see Fig. 3.5a).

(3) Apply inverse transforms (2.115) and (2.114) to find $N(l)$.

3.2 Experimental determination of the existence of oscillatory fine structure

3.2.1 Experiment with polystyrene bead tissue phantom

To confirm the validity of the theory predicting oscillatory fine structure discussed in Chapter 2, the reflectance from a tissue phantom was studied. The phantom consisted of a suspension of polystyrene beads in de-ionized water [Polyscience, Inc.] placed on top of a $BaSO_4$ diffusing (and highly reflective) plate. The bead diameter was l_0= 4.45μm, relative refractive index n=1.19, and the optical distance of the suspension was τ_0=1.06. Thus, every photon underwent approximately one scattering event with a bead while passing through the suspension. The beads were thoroughly mixed with water to exclude the possibility of a number of beads touching each other. Then the beads were allowed to settle. This simulates the conditions in columnar epithelium like that of Barrett's esophagus, colon, or bronchi. This suspension simulated epithelium, with the beads simulating cell nuclei and the $BaSO_4$ plate used to simulate the diffuse reflectance from underlying tissue, such as lamina propria.

In the experiments, an optical fiber probe was used to deliver white light from a xenon arc flashlamp [EC&G] with a 10μsec pulse duration and an average pulse energy of 5J to the phantom and collect the reflectance signal (Fig. 3.3). The probe tip, 1 mm in diameter, consisted of a central delivery fiber surrounded by a ring of six collection fibers, all of which were covered with a 1 mm thick quartz optical shield. The optical fibers were fused silica, 200 μm core diameter, NA=0.22. The tip of the probe was beveled at 17° angle in order to eliminate specular reflection from the shield/air or shield/water interface. At the proximal end of the probe the collection fibers were arranged in a line and imaged onto the input slit of a

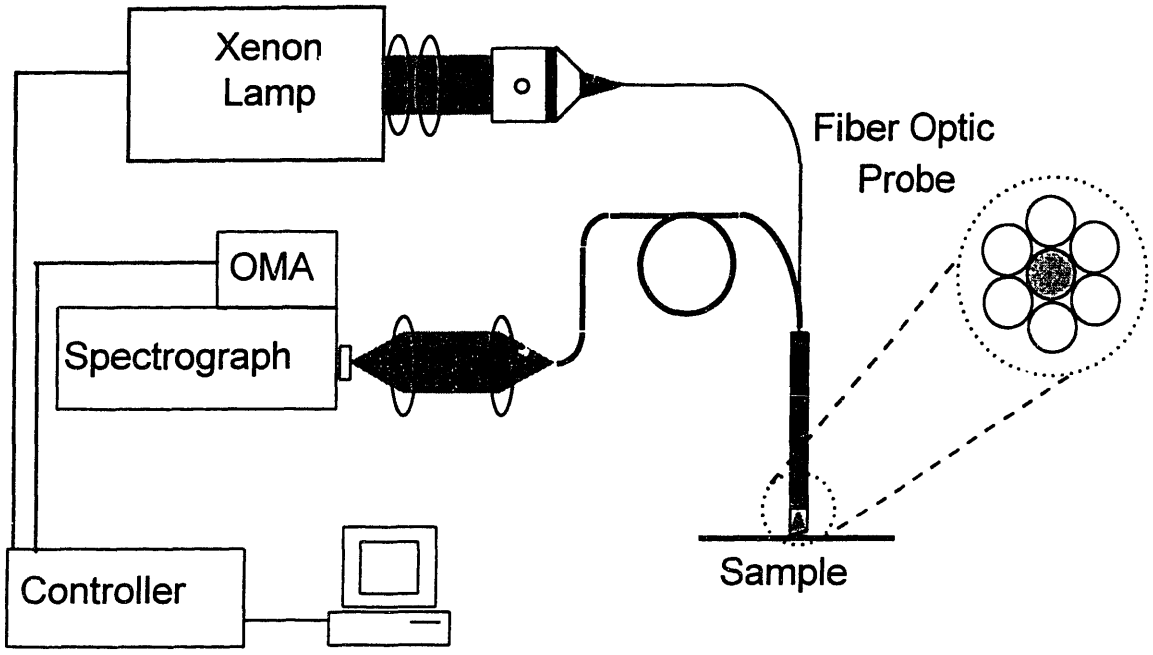

Firure 3.3 The experimental setup.

spectrograph [Instruments SA CP-200], which dispersed the collected light. An electronically gated diode array detector [EG-G PAR OMA III] recorded the reflectance spectra over the wavelength range 360-685 nm. Before data collection, a reference reflectance signal from the $BaSO_4$ plate (without the suspension) was measured. In the experiments, the probe was placed in contact with the suspension.

Fig. 3.4(a) shows the measured reflectance from the phantom. The fine oscillatory component of the signal can be seen. Note that the approximations we made to obtain (2.93) are satisfied by the conditions of this experiment. Expression (2.93) was derived in the following approximations: (1) the particles are large which means $l>>\lambda$ and $\zeta>>1$, (2) the optical distance is not large enough to permit multiple scattering inside the slab, $\tau\leq 1$, (3) the delivery angle and collection angle are small, $\Omega_i<<1$ and $\Omega_c<<1$. In our experiments l was

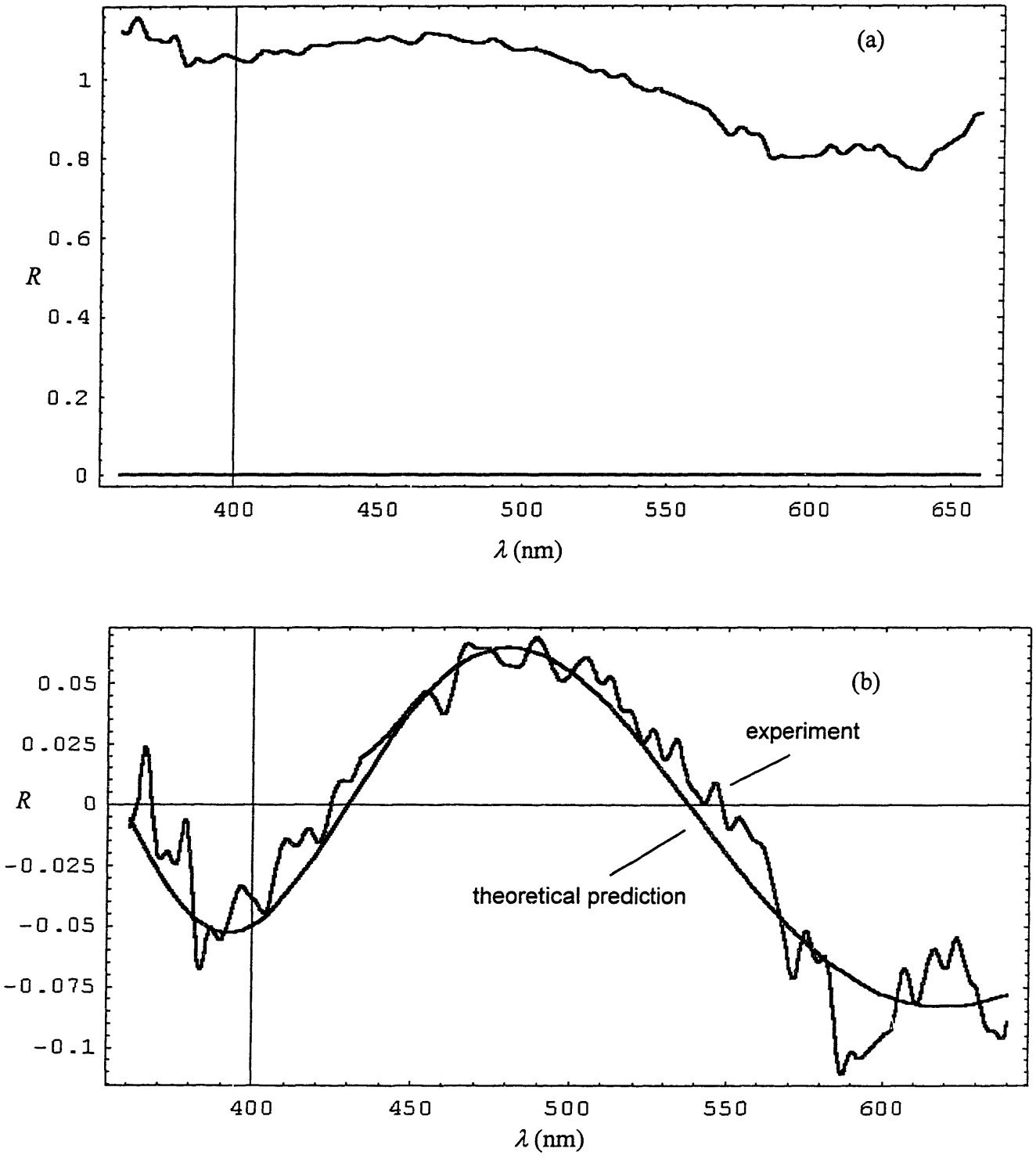

Figurre 3.4 Reflectance from a polysterene bead tissue phantom. (a) – total reflectance; (b) – the oscillatory structure after subtracting out diffuse $BaSo_4$ background.

4.5μm, $\zeta \approx 7$ and condition (1) is satisfied; $\tau_0=1.06$ and condition (2) is satisfied; $\Omega_f=\Omega_c=\pi NA^2=0.15$ and (3) is satisfied. Fig. 3.4(b) shows the ratio $\frac{R(\lambda)}{\overline{R}(\lambda)}$-1 in comparison to the model prediction (2.93). As can be seen, the theory describes the experimental data quite accurately, supporting the validity of the model.

3.2.2 Experiment with cellular monolayers

The experiments with the tissue phantoms described above demonstrate that light scattering by large particles leads to the formation of the oscillatory component in the reflectance. They, however, do not establish that cell nuclei produces in the same effect. To confirm this fact, elastic scattering from cell cultures was studied. The data was collected using the same experimental setup as in the experiments with the tissue phantoms. The samples were monolayers of normal and T84 tumor colonic cells, approximately 15 μm long, affixed to glass slides in buffer solution, and placed on top of a $BaSO_4$ diffusing plate. The tumor cells were grown in a confluent manner. The normal cells were allowed to settle on a glass slide and the remaining nonattached cells were washed out. The diameters of the normal cell nuclei ranged from 5 to 7 μm, and those of the tumor cells from 7 to 16 μm. The cell monolayers simulated epithelium and, like in the experiments with the bead phantoms, the $BaSO_4$ plate simulated the underlying tissues.

Fig. 3.5(a,b) shows the resulting spectra from normal and T84 tumor cell samples, respectively. Distinct spectral features are apparent. For comparison, the reflectance spectrum from the $BaSO_4$ plate by itself is also shown [Fig.3.5(c)]. As can be seen, the latter spectrum lacks structure and shows no prominent features.

The solid curves of Figs. 3.6(a,b) show the resulting nuclear size distributions of the normal and T84 cell culture samples extracted from the spectra of Figures 3.5(a,b) using (2.115). A nuclei-to-cytoplasm relative refractive index of n=1.06 was used. The dashed curves show the corresponding size distributions, measured via light microscopy [15]. The extracted from the spectra and measured via light microscopy distributions can be approximated by Gaussian distributions. The parameters of those are presented in Table 1.

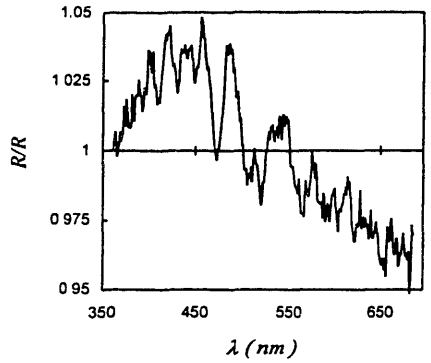

(a)

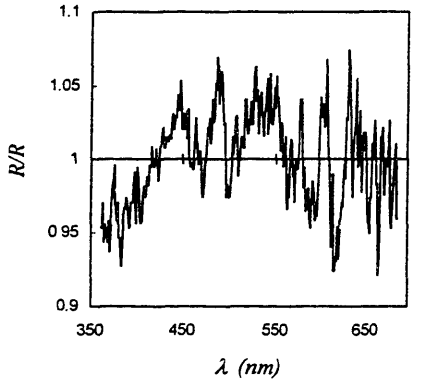

(b)

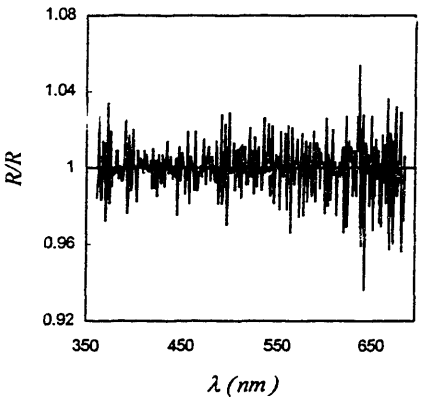

(d)

Figure 3.5 Reflectance spectrum from cell culture monolayer samples. (a) Normal colonic cells ($\overline{R} = 0.38$); (b) T84 cells ($\overline{R} = 0.38$); (c) Reflectance spectrum from the $BaSO_4$ plate.

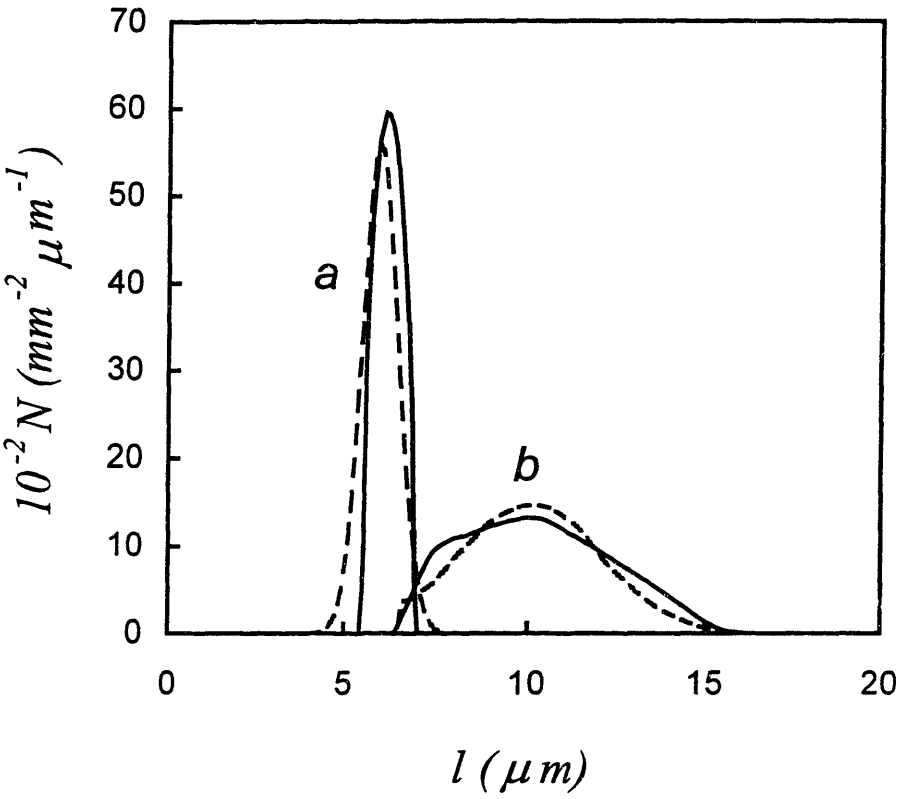

Figure 3.6 Nuclear size distributions from data of Fig. 3.5. (a) Normal colon cells; (b) T84 tumor colonic cells. In each case, the solid line distribution is extracted from the data and the dashed line distribution is measured using light microscopy. Because of insufficient morphometric data, the nuclear size distribution for the normal cell culture sample is depicted as a Gaussian distribution with mean diameter and standard deviation determined from the light microscopy measurements.

As can bee seen, the extracted and measured distributions are in good agreement for both normal and T84 cell samples, indicating the validity of the above picture and the accuracy of our method of extracting the information.

	Normal Cells		Tumor T84 Cells	
	Mean Diameter (μm)	Standard Deviation (μm)	Mean Diameter (μm)	Standard Deviation (μm)
Microscopy	~6	~0.5	10.2	2.0
Spectroscopy	6.2	0.45	10.1	2.2

Table 1 Parameters of nuclear size distributions for normal and T84 tumor colonic cells, measured using light microscopy and extracted from the spectra.

3.3 Clinical experiments. Diagnosis of dysplasia in Barrett's esophagus

We have observed the oscillatory fine structure in diffuse reflectance from esophagus and colon mucosa of patients undergoing gastroenterological endoscopy procedures. We consider here the case of Barrett's esophagus, in which the epithelium consists of a thin monolayer of columnar cells similar to those used in the cell culture experiments. Data was collected as in the cell culture studies. The optical fiber probe was inserted into the biopsy channel of the endoscope and brought into contact with the tissue surface.

Figure 3.7(a) shows the reflectance spectra from two Barrett's esophagus tissue sites, both independently diagnosed by three pathologists as (1) normal and (2) precancerous, i.e. dysplastic. As can be seen, the differences in these unprocessed spectra are small. To analyze them, equation (3.2) was first fit to the broad features of the data by varying the parameters c, α, L, and R_0. The resulting fits are quite accurate. After removing the diffuse background by calculating $R(\lambda)/\overline{R}(\lambda)$, the oscillatory fine structure is seen clearly [Figure 3.7(b)]. In particular, the fine structure from the dysplastic tissue site exhibits higher

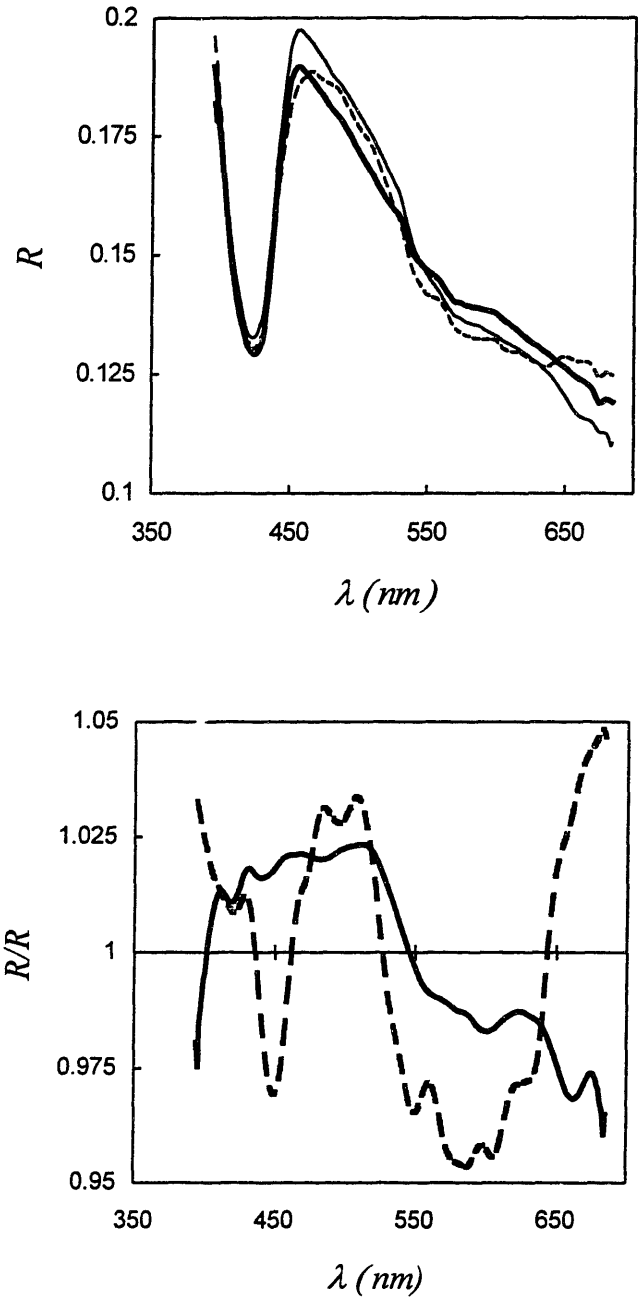

Figure 3.7 Reflectance from Barrett's' esophagus. (a) Diffuse reflectance from non-dysplastic site (solid line), dysplastic site (dashed line), and model fit (thick solid line); (b) corresponding fine structures.

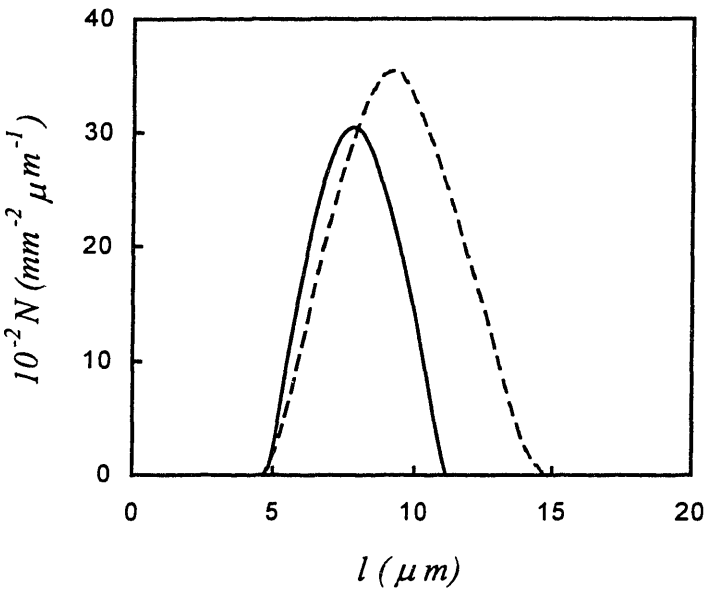

Figure 3.8 Nuclear size distribution obtained from reflectance from Barrett's' esophagus: non-dysplastic site (solid line) and dysplastic site (dashed line).

frequency components than that from the normal site. Transform (2.115) was then employed to extract the respective nuclear size distributions, yielding Figure 3.8. As can be seen, the difference between normal and dysplastic tissue sites is pronounced. The distribution of nuclei from the dysplastic site is much broader than that from the normal site, the peak diameter is shifted from ~7 μm to about ~10 μm, and the shape exhibits distinct structure. In addition, both the relative number of large nuclei (>10 μm) and the total number of nuclei are significantly increased.

This technique was used to study data from 55 tissue sites (9 human subjects). After a reflectance spectrum was measured, biopsy was taken from the same site. The biopsies were independently analyzed by four pathologists. It should be emphasized here that diagnosis of dysplasia in Barrett's esophagus is characterized by significant inter- and intraobserver variability and presents a challenge for even experienced GI pathologists. Agreement between two pathologists on positive diagnosis may be less than 60% [10].

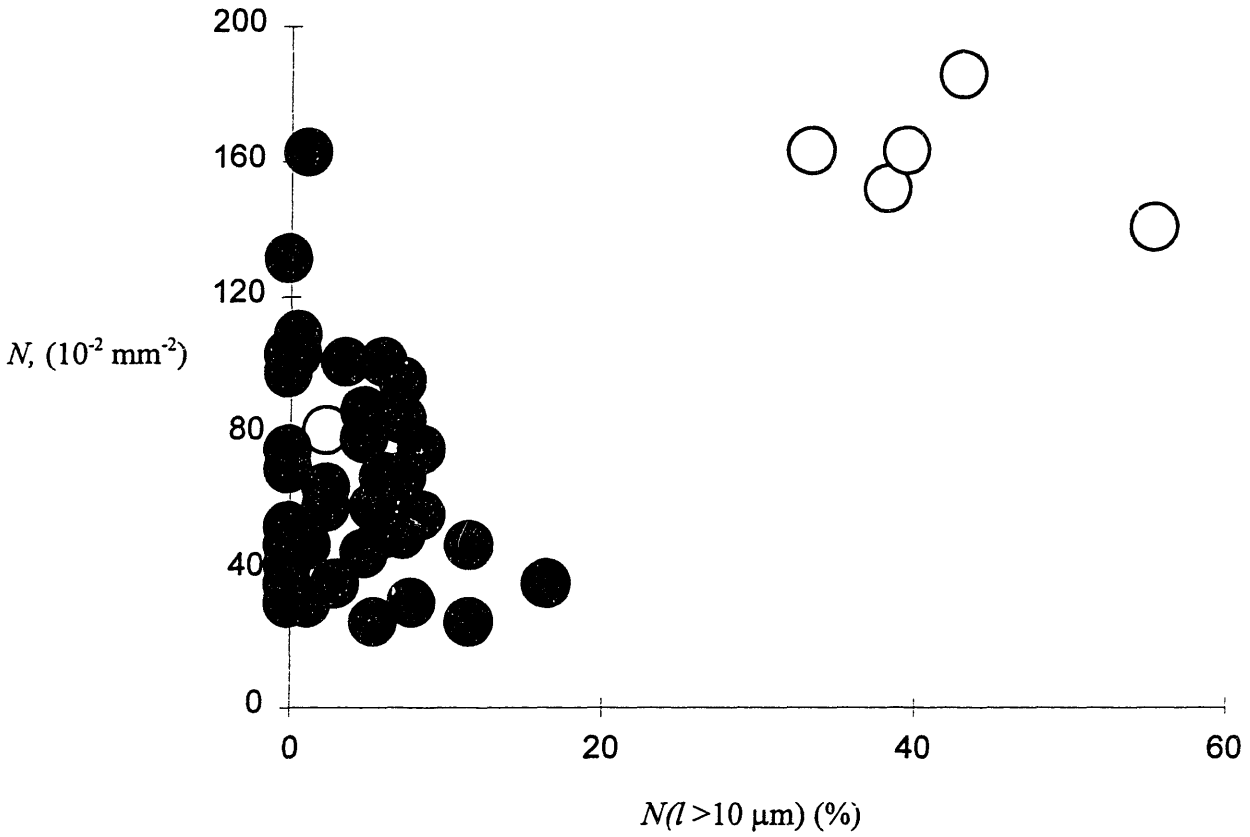

Figure 3.9 Results of clinical studies on patients with Barrett's esophagus. N -- density of epithelial cell nuclei, N(l>10μm) – percentage of nuclei with diameter large 10 μm. Sites diagnosed by all four pathologists as non-dysplastic are represented by dark cycles; those diagnosed at least by three pathologists as "low grade dysplasia" are represented by white cycles.

Therefore, various approaches are possible, including: (1) compare results of "spectroscopy diagnosis" with the averaged score provided by the pathologists and (2) consider only such sites that most/all pathologists agree on the diagnoses. We consider here the second one.

Since most non-dysplastic nuclei range in diameter from 5μm to 8μm, nuclei of regenerating cells can be larger than those of the intact cells but rarely exceed 10μm in diameter, and dysplastic nuclei can easily be larger than 10μm [16]. We therefore define a nucleus with a diameter l>10μm as an "enlarged" and suspected for being dysplastic. As

mentioned above, another important characteristic of the dysplastic epithelium is the stratification and crowding of the nuclei. These properties are reflected by total number of nuclei $N_0 = \int N(l)dl$. A width of a typical non-dysplastic cell is about 12μm. Thus, the non-dysplastic epithelium which does not show stratification contains approximately N_0=70 nuclei per $10^4 \mu m^2$ of surface area. Given that a cell rarely can be smaller than 8μm in diameter, a value of N_0>150nuclei/$10^4 \mu m^2$ is a sign of stratification and crowding.

The resulting plot (total number of nuclei vs. percentage of nuclei with a diameter larger that 10 μm) is presented in Fig. 3.9. Defining dysplastic sites as the ones which have 25% or more of the total number of nuclei larger than 10 μm, the technique diagnosed 35 out of the 36 sites correctly (there was a disagreement among the pathologists regarding other 19 sites), with one dysplastic site out of a total of 6 misidentified. This site could be misidentified because of a number of reasons, including: (1) fault of the technique; (2) the spectrum was taken from a site different from that of the biopsy (sample error); (3) the biopsy was misdiagnosed by the pathologists.

This study suggests that the diagnostic accuracy provided by this technique is at least as good as the accuracy provided by an independent pathologist (more detailed discussion on this issue will be published elsewhere [17]). Additional clinical studies and pathological correlation will be needed to test the applicability of the technique to diagnose dysplastic changes in Barrett's esophagus and other mucosal tissues.

References

1. R.S.Cotran, S.L. Robbins, V. Kumar, *Robbins Pathological Basis of Disease* (W.B. Saunders Company, Philadelphia, 1994).
2. D. W. Fawcett, A Textbook of Histology, (Charman & Hall, New York, 1994).
3. G.I. Zonios, R.M. Cothren, J.T. Arendt, J. Wu, J. Van Dam, J.M. Crawford, R. Manoharan, and M.S. Feld, IEEE Trans. Biomed. Eng. **43**, 113 (1996).
4. G. Zonios, L.T. Perelman, V. Backman, R. Manoharan, J. Van Dam, and M.S. Feld (to be published).
5. L.T. Perelman, V. Backman, M. Wallace, G. Zonios, R. Manoharan, A. Nusrat, S. Shields, M. Seiler, C. Lima, T. Hamano, I. Itzkan, J. Van Dam, J.M. Crawford, and M.S. Feld, Phys.Rev. Lett., **80**, 627 (1998).
6. L.T. Perelman, J. Wu, I. Itzkan and M.S. Feld, Phys. Rev. Lett. **72**, 1341 (1994).
7. J. Wu, M. S. Feld, R. P. Rava, Appl. Opt. **32**, 3585 (1993).
8. P.M. Morse and H. Feshbach, *Methods of Theoretical Physics* (McGraw-Hill, New York, 1953).
9. J.F. Brennan, G.I. Zonios, T.D. Wang, RP Rava, G.B. Hayes, R.R. Dasari, and M.S. Feld, Appl. Spectr. **47**, 2081 (1993).
10. B. Reid, R. Haggitt, Rubin Cea, Human Path., **19**, 166 (1988).
11. G. Zonios, PhD Thesis, MIT, to be published (1998).
12. S.J. Spechler, M.A. Papercorn, J.G. Sweeting, M.I. Burrell, Clinical Teaching Project: Unit 9, Esophageal Disorders (Milner-Fenwick, Inc., Timonium, 1995).

13. A. Ishimaru, Wave Propagation and Scattering in Random Media (Academic Press, Orlando, 1978).

14. R.R. Richards-Kortum, A. Mehta, T. Kolubaev, C. Hoyt, R. Cothren, B. Sacks, C. Kittrell, and M.S. Feld, Laser Spectroscopy, **8**, 336 (1987).

15. Because of insufficient morphometric data, the nuclear size distribution for the normal cell culture sample is depicted as a Gaussian distribution with mean diameter and standard deviation determined from the light microscopy measurements.

16. J. Crowford, R. Mitchell, personal communications.

17. V. Backman, L.T. Perelman, M. Wallace, G. Zonios, R. Manoharan, S. Shields, M. Seiler, I. Itzkan, J. Van Dam, J.M. Crawford, and M.S. Feld, (to be published).

Chapter 4

Conclusions and future directions

4.1 Conclusion

This work has reported observation of a fine structure in light backscattered from biological tissue which is oscillatory in wavelength. The origin of this component is due to light which is Mie-scattered by surface epithelial cell nuclei. It is shown that analyzing the amplitude and frequency of the fine structure, the density and size distribution of these nuclei can be extracted.

The light scattering by a particle large relative to the wavelength was studied. The cross section and phase function of such scatterers were determined in the Van de Hulst approximation. Special attention was given to forward and backward scattering. It was shown that the scattering cross section and other integral characteristics of the light scattering by large particles exhibit oscillatory wavelength dependence.

Knowledge of the properties of the single scattering was then used to study the formation of the reflectance from mucosal tissue. The tissue is modeled by a two layer model. The upper cellular layer (epithelium) was considered as a slab of large particles (cell nuclei) situated on top of a relatively acellular layer (connective and muscular tissues) where light is completely randomized due to diffusion. Light backscattering from a slab of large particles was studied using the first order multiple scattering approximation. Light propagation through the slab was studied using the first order approximation (for a slab of a small thickness) and the small angle multiple scattering

approximation (for a large thickness of the slab). Analytical solutions for the backscatted light and light transmitted through the slab were obtained. It was shown that the reflectance from such a slab has an oscillatory wavelength-dependent component similar to that of the cross section. A transform to invert this oscillatory component to determine the size distribution of the particles in the slab was obtained.

The theoretical predictions were compared to the experiments performed on tissue phantoms and cellular monolayers. The application of the technique to determine epithelial nuclear size distributions in human esophagus was discussed. Since the enlargement of the cell nuclei and their concentration are important indicators of precancerous changes in biological tissue [1], the technique may provide a useful tool for observing such changes in patients. The potential of the technique to diagnose precancerous changes was discussed.

4.2 Future directions

The are three major directions the work could be continued in.

1. Physics related. In the presented work unpolarized white light was used. Instead, it is possible to improve the accuracy and applicability of the technique by using polarized light. This can solve one of the major limitations of the technique – necessity to subtract the diffusive background coming from underepithelial tissues. The illumination of the tissue by polarized light and measuring the dependence of the reflectance not only on the wavelengths but on the polarization state can render the background subtraction much easier and may significantly increase the amplitude of the oscillatory component. Development of the corresponding theoretical apparatus would be necessary. Applicability of some other physical effects such as weak localization can be studied as well.
2. Application related. If the new physical effects which can increase the accuracy and applicability of the technique are found, a new apparatus to diagnose dysplasia in human tissues can be built. New numerical algorithms to analyze the data can be developed. They will be faster and more accurate than the present algorithms.

3. Medically related. More extensive multipatient clinical studies can be performed to test the applicability of this technique to diagnose dysplasia in Barrett's esophagus. So far the technique has been applied to diagnose precancerous changes in human esophagus and colon. Most of the cancers (more than 90%) arise from epithelium. The examples are stomach, mouth, bladder, lung, breast, liver, etc. The technique could be tested on these organs as well. In each case extensive studies are necessary to correlate the results with pathology findings. In the long term prospective, a computer guided biopsy system can be built on the basis of the technique. It can be used as a clinical tool to diagnose dysplastic changes in some of the mentioned organs.

References

1. R.S.Cotran, S.L. Robbins, V. Kumar, *Robbins Pathological Basis of Disease* (W.B. Saunders Company, Philadelphia, 1994).